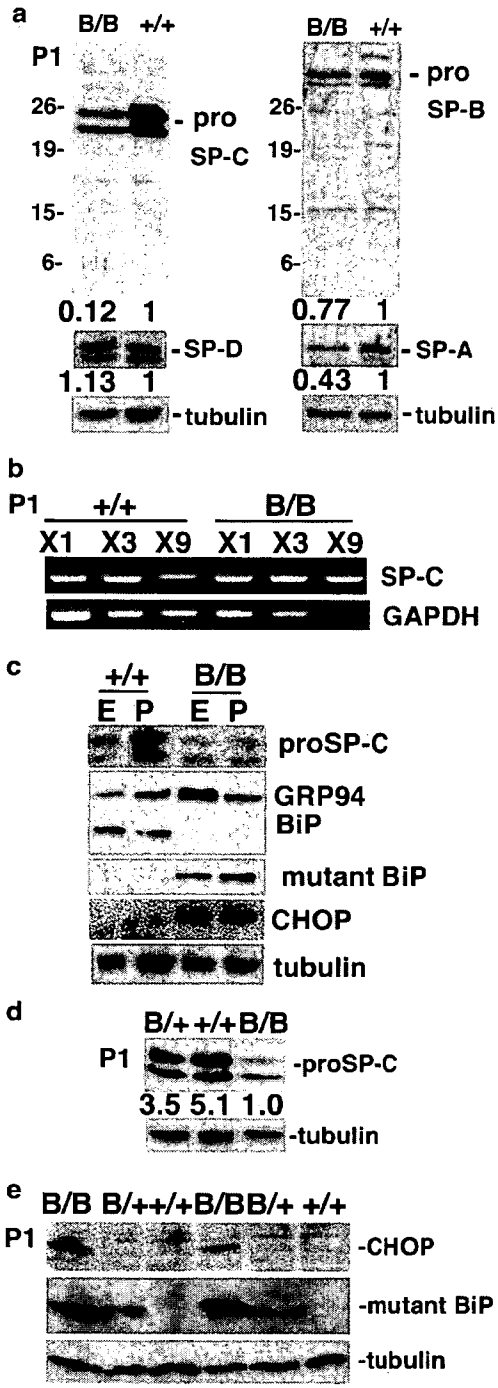

Figure 6 Biosynthesis of pulmonary surfactant is impaired in mutant-BiP lung. (**a**) Western blots of SP-A, SP-B (proSP-B), SP-C (proSP-C), SP-D and γ-tubulin in lungs from P1 wild types ($+/+$) and mutants (B/B). The expression of each protein was normalized to that of γ-tubulin. (**b**) SP-C mRNA in lungs from P1 wild-types ($+/+$) and mutants (B/B) was evaluated by semi-quantitative RT-PCR. Serial dilutions of cDNA were standardized to GAPDH. (**c**) Western blots of pro-SP-C, GRP94, BiP, mutant BiP, CHOP, and γ-tubulin in lungs from E18.5 (E) and P1 (P) mice. (**d**) Western blots of SP-C (proSP-C) and γ-tubulin in lungs from P1 wild-type ($+/+$), heterozygous (B/ $+$), and homozygous (B/B) mutant mice. The expression of SP-C was normalized to that of γ-tubulin. (**e**) Western blots of mutant BiP, CHOP, and γ-tubulin in P1 lungs

secretion into alveolar space via regulated exocytosis. Lamellar body formation is defective in alveolar type II cells of neonatal BiP mutants. Therefore, SP-C may be degraded by endosomal/lysosomal degradation and/or the ERAD pathway. Punctate SP-C is colocalized with KDEL-containing ER chaperones in both wild-type and homozygous mutant type II cells (Figure 9a), suggestive of ER accumulation of SP-C. The fraction of ER accumulation of SP-C in the mutant type II cells was 0.84, while that of Golgi accumulation was 0.08, evaluated by confocal colocalization images (Figure 9a and b).

To examine the effect of proteasome inhibitors on SP-C, MEFs from wild-type and homozygous mutant embryos were transfected with SP-C in the presence or absence of a proteasome inhibitor (Figure 9c and d). Although the proteasome inhibitor enhanced SP-C expression in wild-type and BiP mutant MEFs, it enhanced surface expression of SP-C in wild-type MEFs but promoted ER accumulation of SP-C in the BiP mutant MEFs. Although endosomal/lysosomal degradation of SP-C cannot be excluded, these data suggest that, in homozygous mutant-BiP type II cells, misfolded SP-C may accumulate in the ER and be degraded by the ERAD pathway.

Discussion

We produced knock-in mice expressing a mutant BiP lacking the retrieval sequence to examine the effects of defects in the secretory pathway stress response without completely eliminating BiP function—as would be the case in BiP knockout mice.[21] Mutant BiP predominantly affected dedicated secretory cells, such as alveolar type II cells, in which active secretion is particularly important. Putative impairment of protein folding in these mutant cells probably caused the observed respiratory failure and high neonatal mortality.

Deletion of the retrieval sequence from BiP, and the consequent lack of mutant-BiP recycling, could have two possible effects. First, the folding environment in the ER may be impaired. However, mutant BiP is functional as long as it remains in the ER. Therefore, constitutive activation of the UPR could compensate for the altered folding environment by producing mutant BiP in quantities sufficient for cell survival. Second, quality control in post-ER compartments may be affected. Proper ER-to-Golgi transport and subsequent ER retrieval of proteins and lipids is thought to contribute to quality control.[16,17,23] In this regard, the folding (and therefore function) of pulmonary SPs, especially proSP-C, may depend on proper ER retrieval of BiP via the KDEL receptor.

Respiratory distress syndrome of newborns, also called hyaline membrane disease, causes high mortality and often accompanies pre-term delivery or low birth weight with reduced expression of pulmonary surfactant. Surfactant therapy combined with mechanical ventilation and other intensive care measures has reduced the mortality rate of this syndrome to below 10%.[24] Surfactant proteins are required for proper lung development and function. Respiratory diseases result in humans and other mammals when these proteins are lacking. SP-B is critical for lung surfactant formation and function, and its deficiency causes immediate and severe neonatal respiratory failure in humans and mice.[25,26] Deletion of SP-B induces aberrant processing of proSP-C as well as defects in lamellar body formation. SP-C

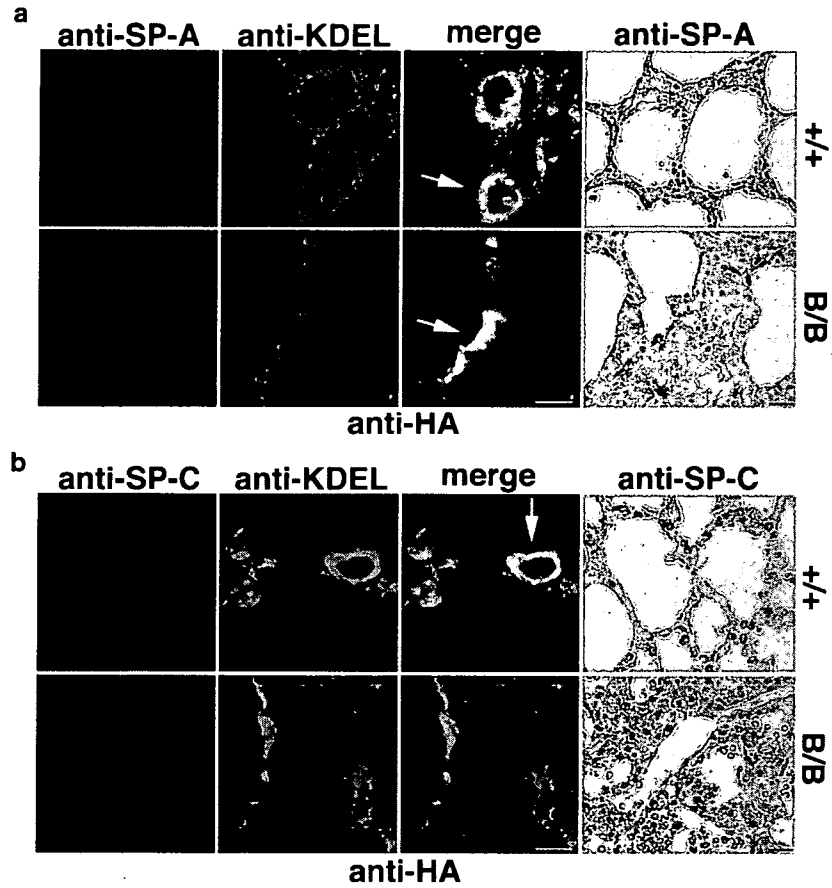

Figure 7 SP-A and SP-C in lungs from BiP mutants. (**a**) Costaining of lungs from P1 wild-type (+/+) and mutant (B/B) mice with anti-SP-A (brown staining, right panels) and monoclonal anti-KDEL or anti-HA (shown in green in different panels). (**b**) Costaining of lungs from P1 wild types (+/+) and mutants (B/B) with anti-SP-C (proSP-C; right panels) and anti-KDEL or anti-HA. Arrows indicate colocalization of SP-A or SP-C with KDEL-containing chaperones in wild-type type II cells as well as colocalization of SP-A with mutant BiP in B/B type II cells

deficits are related to acute and chronic infant lung diseases in humans[27] and respiratory failure in cattle.[28] Furthermore, mutations in proSP-C have been correlated with chronic interstitial pneumonia.[11,12] ProSP-C is an type II integral membrane protein with structural homology to the amyloidogenic BRI family of proteins, which cause neurodegenerative dementia.[29] Mutant proSP-C tends to misfold and may cause protein aggregation and ER stress.[12] Thus, in the present study, aberrant quality control in the mutant-BiP type II epithelial cells may have resulted in proSP-C misfolding. Misfolded proSP-C may act in concert with decreased pulmonary surfactant levels to generate respiratory failure by causing ER stress in mutant type II cells.

Mutant-BiP mice have a distinct phenotype, as is the case for mice lacking other ER molecular chaperones. Hsp47 is responsible for collagen biosynthesis, and Hsp47 knockout mice die on E11.5.[30] Calreticulin and calnexin participate in glycoprotein folding in the ER. Calreticulin knockout mice are embryonic lethal and display defective cardiac development.[31] Calnexin knockout mice die during the early postnatal period, between birth and 3 months of age. These mice exhibit motor disorders owing to a loss of large myelinated nerve fibers.[32]

The UPR is a ubiquitous mechanism for adapting to ER stress, and BiP is an essential component of this system. However, at various developmental stages, some cell types require specific UPR signaling systems[33] and chaperones. Mutant mouse models have revealed that the UPR plays a vital role during development by increasing protein synthesis as needed in dedicated secretory cells,[34] such as pancreatic β cells,[35] plasma cells[36] and hepatocytes.[37] Inadequate adaptation to these types of physiological demands may lead to diverse diseases.

Diminished quality control in the ER and in post-ER compartments of the mutant-BiP alveolar type II cells may be sufficient embryonically but not neonatally when increased biosynthesis of proSP-C and other SPs requires sufficient folding capacity. Indeed, at E18.5, proSP-C expression in type II cells was equivalent in lungs from BiP mutants and wild types (Figures 5b and 6c). After birth, proSP-C expression increased markedly in wild-type lungs but not in mutant lungs. SP-C mRNA level was, however, preserved in the BiP mutants, suggesting that proSP-C may be degraded co- or post-translationally in neonatal mutants.

Our results suggest that in neonates a physiological increase in SP production causes ER stress in dedicated secretory cells, like alveolar type II epithelial cells. This may increase susceptibility to environmental insults such as hypoxia and ischemia, leading to respiratory failure due to the

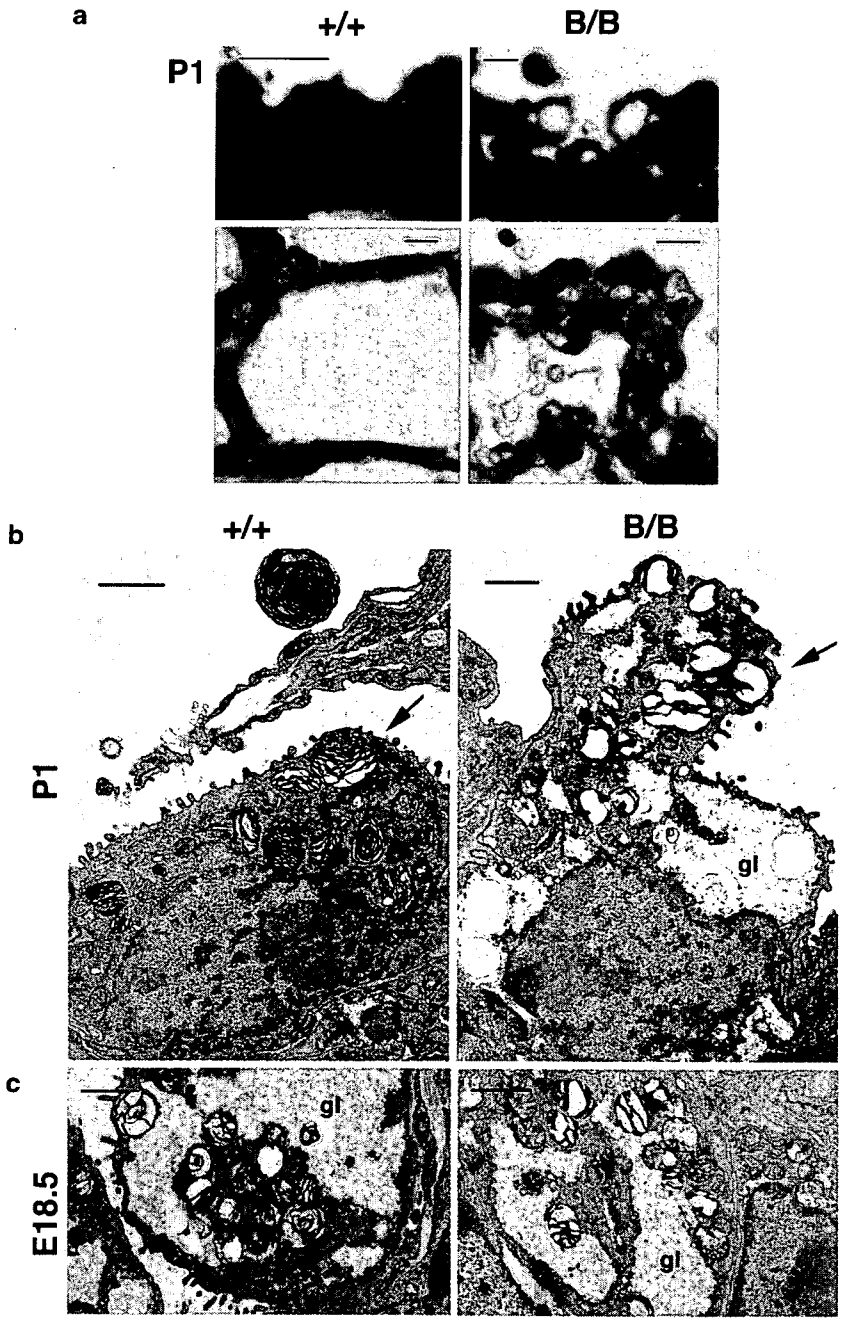

Figure 8 Defective lamellar body formation in neonatal mutant-BiP alveolar type II cells. (**a**) Neonatal mutant type II cells contained vacuole structures. Alveolar epithelium from P1 wild type (+/+) and mutant (B/B) mice stained with toluidine blue (upper panels) or PAS (lower panels). Scale bars represent 10 μm. (**b**, **c**) Ultrastructure of the alveolar epithelium from wild type (+/+) and mutant-BiP (B/B) P1 neonates (**b**) and E18.5 embryos (**c**). Scale bars represent 1 μm. Arrows indicate lamellar bodies in type II cells. Cytoplasmic glycogen (gl) remained in neonatal mutant type II cells.

loss of pulmonary surfactant and accumulation of misfolded proteins in the ER.

Materials and Methods

Cells, reagents, and general procedures. MEFs were prepared from E13.5 embryos. MEFs were grown at 37°C in an atmosphere of 5% CO_2 in complete medium consisting of Dulbecco's modified essential medium (DMEM; Sigma Chemical Co.) with 15% fetal bovine serum (FBS), 2 mM glutamine, 50 μg ml^{-1} streptomycin and 50 U ml^{-1} penicillin G.

The following antibodies were used: rabbit antiserum against calreticulin (Affinity Bioreagent), rabbit antiserum against XBP-1, rabbit antiserum against ATF4, rabbit antiserum against CHOP/GADD153, goat polyclonal antiserum against BiP/GRP78, rabbit antiserum against SP-A (H-148), goat polyclonal antiserum against SP-B (R-19), rabbit antiserum against SP-C (FL-197), rabbit antiserum against SP-D (C-18), rabbit antiserum against ubiquitin (all from Santa Cruz Biotechnology), rabbit anti-serum against the HA epitope (Zymed), mouse monoclonal antibody (mAb) against γ-tubulin (Sigma Chemical), mouse mAb SPA-827 against BiP (KDEL sequence; Stressgen), mouse mAb G1/133 against giantin (Alexis Biochemicals), Cy-2- or Cy-3-conjugated donkey antibody against rabbit IgG, and Cy-2- or

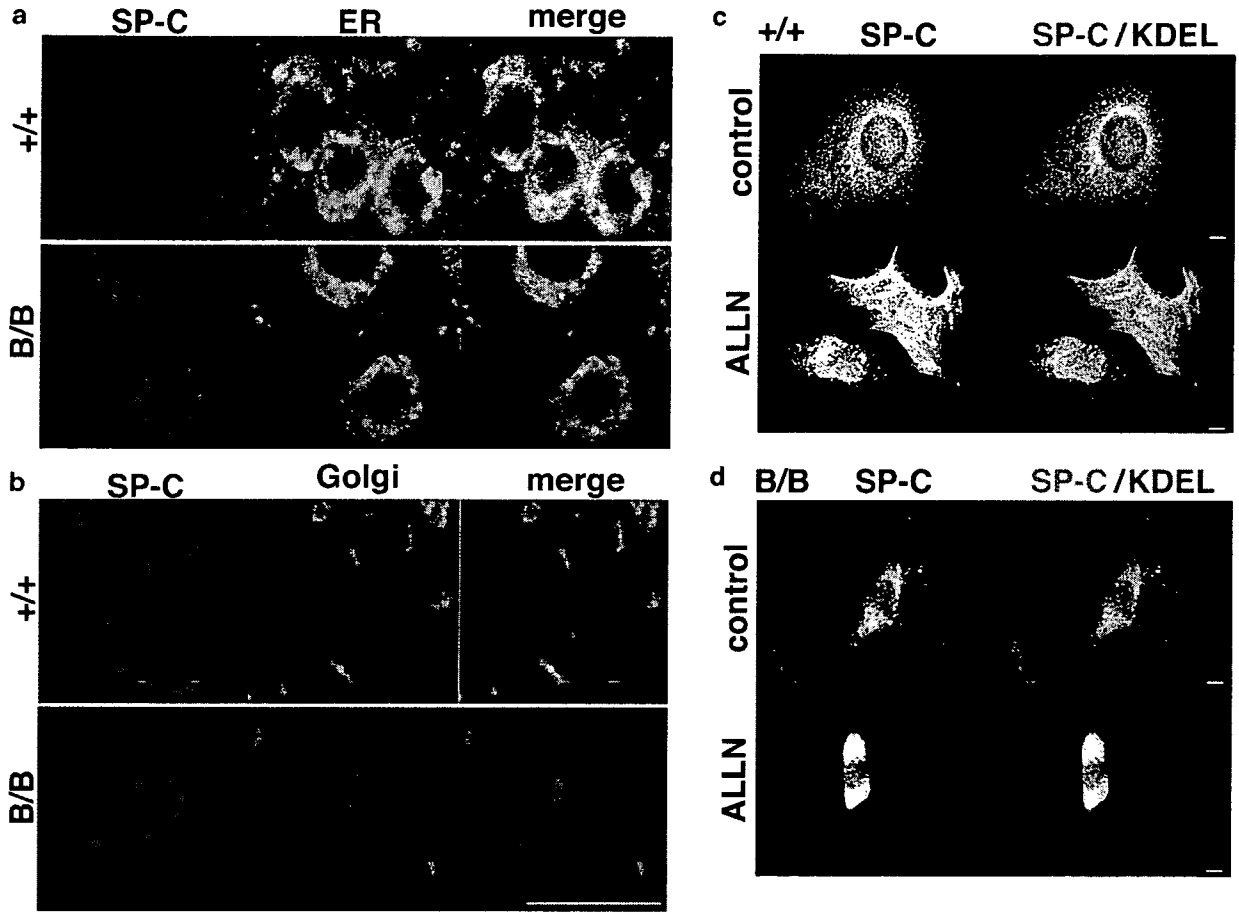

Figure 9 SP-C accumulation in the ER. (**a**) Lungs from a P1 wild-type neonate (+/+) and a homozygous mutant (B/B) costained with polyclonal anti-SP-C and monoclonal anti-KDEL (ER staining). Colocalization of SP-C with KDEL-containing ER chaperones was seen in both wild type and mutant alveolar type II cells. (**b**) Lungs from a P1 wild-type neonate (+/+) and a homozygous mutant (B/B) co-stained with polyclonal anti-SP-C and monoclonal anti-giantin (Golgi complex staining). Scale bar represents 10 μm. The fractions of ER-localizing SP-C and Golgi-localizing SP-C were calculated by confocal colocalization images. ER-localizing SP-C to total SP-C in wild type; 0.81 ± 0.052, Golgi-localizing SP-C in wild type; 0.12 ± 0.032, ER-localizing SP-C in mutant; 0.84 ± 0.036 (significantly more than that of wild types by *t*-test, $P < 0.018$), Golgi-localizing SP-C in mutant; 0.08 ± 0.043 (significantly less than that of wild types, $P < 0.0015$). $n = 20$, mean $\pm$ S.D. (**c**, **d**) Inhibition of proteasomal degradation promotes ER accumulation of SP-C in homozygous mutant MEFs. MEFs from wild type (+/+, **c**) and homozygous mutant (B/B, **d**) embryos were transfected with SP-C with or without ALLN (10 μg ml^{-1}; 12 h) then double-stained with monoclonal anti-KDEL (red) and polyclonal anti-SP-C (green). Anti-KDEL recognizes BiP as well as other KDEL-containing proteins, such as GRP94. Scale bars represent 10 μm

Cy-3-conjugated donkey antibody against mouse IgG (Jackson Immunoresearch Laboratories). Tunicamycin was purchased from Nacali Tasque. Perfluorocarbon (perfluoro-2-butyltetrahydrofuran) was purchased from Fluorochem. *N*-acetyl-l-leucinal-l-lecinal-l-norleucinal (ALLN) was purchased from Sigma Chemical.

Metabolic labeling experiments and Western blotting were performed as described previously.[6] Densitometry was performed using BAS 2500 and Image Gauge software (Fuji Photo Film Co., Ltd.) for metabolic labeling experiments and using LAS 1000 (Fuji Photo Film Co., Ltd.) and ImageJ software (Wayne Rasband, NIH) for Western blotting.

Generating mutant-BiP mice. All animal experimental procedures were in accordance with a protocol approved by the Institutional Animal Care Committee of Chiba University, Chiba, Japan. A rat BiP cDNA was used as a probe to isolate a genomic clone containing the whole exon of the BiP gene[38] from the 129/SvJ mouse genomic library in λFIXII (Stratagene). A 0.6-kb *Bam*HI/*Xho*I fragment encoding the C-terminal end of BiP and the stop codon, but lacking the KDEL sequence, was obtained by PCR. Then, part of a 2.1-kb genomic fragment containing the last three exons was replaced by the 0.6-kb fragment. The resultant fragment was used as a short arm for the targeting vector. A 0.5-kb *Xba*I/*Kpn*I fragment, encoding the 3′ untranslated region of the exon after the stop codon and the 2.5-kb intron that followed, was amplified by a PCR and used as a long arm for the targeting vector. An *Xho*I/*Xba*I fragment containing a neomycin selection cassette flanked by *loxP* sequences (PHR68, a gift from T Kondo, Saitama, Japan) and a 2.7-kb fragment containing the HSV-thymidine kinase gene were introduced into the targeting vector to allow negative and positive selection. The targeting vector was linearized with *Not*I digestion and used for electroporation into R1 ES cells. The mutant allele resulting from homologous recombination had artificial *Xho*I and *Xba*I sites. Genomic DNA from G418-resistant clones (G418 was from Life Technologies) was digested with *Xba*I and analyzed by Southern blotting using an *Xba*I/*Hin*dIII fragment for the 5′-end probe and a PCR-amplified fragment for the 3′-end probe, as shown in Figure 1. Several homologous recombinants were obtained, and germline chimeras were generated as described.[39] Resulting male chimeras were mated to C57BL/6 females. Tail DNA from the offspring was screened by PCR using the following oligonucleotides: 5′-gatcagtgcacctacaactc-3′ and 5′-gctcaaagagcgcattgac-3′ for the wild-type allele, and 5′-gtgaacgacccctaacaa aa-3′ and 5′-agcgtaatctggaacatcgt-3′ for the recombinant allele. To remove the neomycin selection cassette, heterozygous mice were mated with mice expressing Cre under the control of a CAG promoter. Heterozygous mice lacking neomycin were interbred to obtain homozygous mutant mice.

Detection of mRNA. Northern blot analysis was carried out as described.[6] Expression of BiP and β-actin mRNAs was evaluated using cDNA probes encoding rat BiP (a gift from Dr. HRB Pelham) and mouse β-actin. Radioactivity was

measured using BAS 2500 and Image Gauge software (Fuji Photo Film Co. Ltd.). The expression of BiP mRNA was normalized to that of β-actin. RT-PCR analysis was performed with the following primers: 5′-acctcaaacgccttctcatc-3′ and 5′-tttctgg gcaggagcagctt-3′ for SP-C, and 5′-atggggtgaggccggtgctg-3′ and 5′-cttgatgtcatcata cttgg-3′ for GAPDH.

Whole-mount *in situ* hybridization. Whole-mount *in situ* hybridization was performed using digoxigenin-labeled riboprobes as described[40] with rat BiP cDNA.

Transfection. A cDNA encoding mouse SP-C was obtained from wild-type lung mRNA using the following primers: 5′-ccttacaaaatggacatgag-3′ and 5′-cggatccacga tatagtagagtggtagct-3′. The cDNA was subcloned into a pcDNA3.1 myc-His vector (Invitrogen). The DNA sequence was verified using the Applied Biosystems ABI Prism 310 genetic analyzer. Transfection was performed with Fugene 6 (Roche).

Histochemistry. Lungs were isolated and fixed in 4% paraformaldehyde for 24 h. After fixation, they were dehydrated in increasing concentrations of ethanol and embedded in paraffin wax. Sections (8 m) were stained with hematoxylin and eosin. For immunohistochemistry, sections were incubated with 10% normal goat or bovine serum in phosphate-buffered saline (PBS) for 30 min to block non-specific antibody binding, and then incubated with a primary antibody in PBS for 12 h at 4°C. Sections were rinsed with PBS, incubated with a secondary antibody in PBS for 2 h at room temperature and then visualized using the VECTASTAIN Elite ABC kit (Vector Laboratories) with diaminobenzidine (Sigma).

Confocal and immunofluorescence microscopy. Cells on coverslips were fixed in 2% formaldehyde in PBS for 10 min at room temperature and then processed as described.[6] Labeled cells were examined using a confocal laser scanning microscope (Axiovert 100M, LSM510, Ver. 3.2, Carl Zeiss) fitted with krypton and argon lasers and a Plan-Apochromat 100 NA 1.40 oil immersion objective.

Electron microscopy. Fifteen newborn animals and 24 embryos were processed for electron microscopy. Newborn animals were fixed within 2 h of birth. Embryos were fixed on E18.5. Before fixation, a tail sample was collected for genotyping.

Animals were anesthetized on ice. The thorax was opened, and the heart was removed with part of the large vessels. The trachea was clamped with tweezers, and both the left and right lobes of the lung were excised after cutting the trachea just proximal to the clamped site. The lung was immediately placed in a syringe filled with 3% glutaraldehyde in 10 mM HEPES, 145 mM NaCl (pH 7.4). After the air in the lung and air ducts was expelled by manipulating the plunger, the lung was cut into small pieces with a razor blade and was further fixed in the same fixative for an additional 2 h. After postfixation with 1% osmium tetroxide, the tissue was dehydrated in absolute ethanol and embedded in Epon mixture (TAAB, Berks, England). Ultra-thin sections, double-stained with uranyl acetate and lead citrate, were observed using an electron microscope (1200EX-II, JEOL, Tokyo, Japan).

Statistical analysis. Statistical analyses were performed by one-way analysis of variance and the Bonferroni test and *t*-test using KaleidaGraph software (Synergy Software, Reading, PA, USA).

Acknowledgements. We thank Dr. T Nishino for critical comments. We also thank R Kimura and R Fujii for excellent technical assistance. This work was supported by Grants-in-Aid for Science Research from the Ministry of Education, Culture, Sports, Science and Technology to TA.

1. Ellgaard L, Helenius A. Quality control in the endoplasmic reticulum. *Nat Rev Mol Cell Biol* 2003; **4**: 181–191.
2. Patil C, Walter P. Intracellular signaling from the endoplasmic reticulum to the nucleus: the unfolded protein response in yeast and mammals. *Curr Opin Cell Biol* 2001; **13**: 349–355.
3. Schroder M, Kaufman RJ. The Mammalian unfolded protein response. *Annu Rev Biochem* 2005; **74**: 739–789.
4. Kopito RR, Ron D. Conformational disease. *Nat Cell Biol* 2000; **2**: E207–E209.
5. Kaufman RJ. Orchestrating the unfolded protein response in health and disease. *J Clin Invest* 2002; **110**: 1389–1398.
6. Hamada H, Suzuki M, Yuasa S, Mimura N, Shinozuka N, Takada Y *et al.* Dilated cardiomyopathy caused by aberrant endoplasmic reticulum quality control in mutant KDEL receptor transgenic mice. *Mol Cell Biol* 2004; **24**: 8007–8017.
7. Oyadomari S, Koizumi A, Takeda K, Gotoh T, Akira S, Araki E *et al.* Targeted disruption of the Chop gene delays endoplasmic reticulum stress-mediated diabetes. *J Clin Invest* 2002; **109**: 525–532.
8. Clark H, Clark LS. The genetics of neonatal respiratory disease. *Semin Fetal Neonatal Med* 2005; **10**: 271–282.
9. Korimilli A, Gonzales LW, Guttentag SH. Intracellular localization of processing events in human surfactant protein B biosynthesis. *J Biol Chem* 2000; **275**: 8672–8679.
10. Mulugeta S, Nguyen V, Russo SJ, Muniswamy M, Beers MF. A surfactant protein C precursor protein BRICHOS domain mutation causes endoplasmic reticulum stress, proteasome dysfunction, and caspase 3 activation. *Am J Respir Cell Mol Biol* 2005; **32**: 521–530.
11. Bridges JP, Xu Y, Na CL, Wong HR, Weaver TE. Adaptation and increased susceptibility to infection associated with constitutive expression of misfolded SP-C. *J Cell Biol* 2006; **172**: 395–407.
12. Beers MF, Mulugeta S. Surfactant protein C biosynthesis and its emerging role in conformational lung disease. *Annu Rev Physiol* 2005; **67**: 663–696.
13. Hendershot LM. The ER function BiP is a master regulator of ER function. *Mt Sinai J Med* 2004; **71**: 289–297.
14. Sonnichsen B, Fullekrug J, Nguyen Van P, Diekmann W, Robinson DG, Mieskes G. Retention and retrieval: both mechanisms cooperate to maintain calreticulin in the endoplasmic reticulum. *J Cell Sci* 1994; **107**: 2705–2717.
15. Bertolotti A, Zhang Y, Hendershot LM, Harding HP, Ron D. Dynamic interaction of BiP and ER stress transducers in the unfolded- protein response. *Nat Cell Biol* 2000; **2**: 326–332.
16. Hammond C, Helenius A. Quality control in the secretory pathway: retention of a misfolded viral membrane glycoprotein involves cycling between the ER, intermediate compartment, and Golgi apparatus. *J Cell Biol* 1994; **126**: 41–52.
17. Yamamoto K, Fujii R, Toyofuku Y, Saito T, Koseki H, Hsu VW *et al.* The KDEL receptor mediates a retrieval mechanism that contributes to quality control at the endoplasmic reticulum. *EMBO J* 2001; **20**: 3082–3091.
18. Munro S, Pelham HR. A C-terminal signal prevents secretion of luminal ER proteins. *Cell* 1987; **48**: 899–907.
19. Lewis MJ, Pelham HR. A human homologue of the yeast HDEL receptor. *Nature* 1990; **348**: 162–163.
20. Beh CT, Rose MD. Two redundant systems maintain levels of resident proteins within the yeast endoplasmic reticulum. *Proc Natl Acad Sci USA* 1995; **92**: 9820–9823.
21. Luo S, Mao C, Lee B, Lee AS. GRP78/BiP is required for cell proliferation and protecting the inner cell mass from apoptosis during early mouse embryonic development. *Mol Cell Biol* 2006; **26**: 5688–5697.
22. Zinszner H, Kuroda M, Wang X, Batchvarova N, Lightfoot RT, Remotti H *et al.* CHOP is implicated in programmed cell death in response to impaired function of the endoplasmic reticulum. *Genes Dev* 1998; **12**: 982–995.
23. Taxis C, Vogel F, Wolf DH. ER-golgi traffic is a prerequisite for efficient ER degradation. *Mol Biol Cell* 2002; **13**: 1806–1818.
24. Hallman M. Lung surfactant, respiratory failure, and genes. *N Engl J Med* 2004; **350**: 1278–1280.
25. Nogee LM, de Mello DE, Dehner LP, Colten HR. Brief report: deficiency of pulmonary surfactant protein B in congenital alveolar proteinosis. *N Engl J Med* 1993; **328**: 406–410.
26. Clark JC, Wert SE, Bachurski CJ, Stahlman MT, Stripp BR, Weaver TE *et al.* Targeted disruption of the surfactant protein B gene disrupts surfactant homeostasis, causing respiratory failure in newborn mice. *Proc Natl Acad Sci USA* 1995; **92**: 7794–7798.
27. Lahti M, Marttila R, Hallman M. Surfactant protein C gene variation in the Finnish population – association with perinatal respiratory disease. *Eur J Hum Genet* 2004; **12**: 312–320.
28. Danlois F, Zaltash S, Johansson J, Robertson B, Haagsman HP, van Eijk M *et al.* Very low surfactant protein C contents in newborn Belgian White and Blue calves with respiratory distress syndrome. *Biochem J* 2000; **351** (Part 3): 779–787.
29. Kim SH, Creemers JW, Chu S, Thinakaran G, Sisodia SS. Proteolytic processing of familial British dementia-associated BRI variants: evidence for enhanced intracellular accumulation of amyloidogenic peptides. *J Biol Chem* 2002; **277**: 1872–1877.
30. Nagai N, Hosokawa M, Itohara S, Adachi E, Matsushita T, Hosokawa N *et al.* Embryonic lethality of molecular chaperone hsp47 knockout mice is associated with defects in collagen biosynthesis. *J Cell Biol* 2000; **150**: 1499–1506.
31. Mesaeli N, Nakamura K, Zvaritch E, Dickie P, Dziak E, Krause KH *et al.* Calreticulin is essential for cardiac development. *J Cell Biol* 1999; **144**: 857–868.
32. Denzel A, Molinari M, Trigueros C, Martin JE, Velmurgan S, Brown S *et al.* Early postnatal death and motor disorders in mice congenitally deficient in calnexin expression. *Mol Cell Biol* 2002; **22**: 7398–7404.
33. Zhang K, Shen X, Wu J, Sakaki K, Saunders T, Rutkowski DT. Endoplasmic reticulum stress activates cleavage of CREBH to induce a systemic inflammatory response. *Cell* 2006; **124**: 587–599.
34. Wu J, Kaufman RJ. From acute ER stress to physiological roles of the unfolded protein response. *Cell Death Differ* 2006; **13**: 374–384.

35. Scheuner D, Song B, McEwen E, Liu C, Laybutt R, Gillespie P. Translational control is required for the unfolded protein response and *in vivo* glucose homeostasis. *Mol Cell* 2001; **7**: 1165–1176.
36. Reimold AM, Iwakoshi NN, Manis J, Vallabhajosyula P, Szomolanyi-Tsuda E, Gravallese EM. Plasma cell differentiation requires the transcription factor XBP-1. *Nature* 2001; **412**: 300–307.
37. Reimold AM, Etkin A, Clauss I, Perkins A, Friend DS, Zhang J. An essential role in liver development for transcription factor XBP-1. *Genes Dev* 2000; **14**: 152–157.
38. Haas IG. and Meo T cDNA cloning of the immunoglobulin heavy chain binding protein. *Proc Natl Acad Sci USA* 1988; **85**: 2250–2254.
39. Nagy A, Rossant J, Nagy R, Abramow-Newerly W, Roder JC. Derivation of completely cell culture-derived mice from early-passage embryonic stem cells. *Proc Natl Acad Sci USA* 1993; **90**: 8424–8428.
40. Wilkinson DG, Nieto MA. Detection of messenger RNA by *in situ* hybridization to tissue sections and whole mounts. *Methods Enzymol* 1993; **225**: 361–373.

DEVELOPMENTAL DYNAMICS 236:1484–1494, 2007

SPECIAL ISSUE RESEARCH ARTICLE

Transcription Factors Mesp2 and Paraxis Have Critical Roles in Axial Musculoskeletal Formation

Yu Takahashi,[1]* Atsuya Takagi,[1] Shuichi Hiraoka,[2] Haruhiko Koseki,[2] Jun Kanno,[1] Alan Rawls,[3] and Yumiko Saga[4]

Mesp2 **and** ***Paraxis*** **are basic helix–loop–helix (bHLH) -type transcription factors coexpressed in the presomitic mesoderm (PSM) and are required for normal somite formation. Here, we show that** ***Mesp2/Paraxis*** **double-null mice exhibit a distinct phenotype unexpected from either** ***Mesp2*** **or** ***Paraxis*** **single-null mice. In the posterior region of the body, most of the skeletal components of both the vertebral body and neural arches are severely reduced and only a rudimental lamina and ribs remain, indicating a strong genetic interaction in the sclerotomal cell lineage. However, yeast two-hybrid analyses revealed no direct interaction between Mesp2 and Paraxis. The** ***Mesp2/Paraxis*** **double-null embryo has caudalized somites, revealed by expanded** ***Uncx4.1*** **expression pattern observed in the** ***Mesp2*** **-null embryo, but the expression level of** ***Uncx4.1*** **was significantly decreased in mature somites, indicative of hypoplasia of lateral sclerotome derivatives. By focusing on vertebral column formation, we found that expressions of** ***Pax1, Nkx3.1,*** **and** ***Bapx1*** **are regulated by Paraxis and that Pax9 expression was severely affected in the** ***Mesp2/Paraxis*** **double-null embryo. Furthermore, the expression of** ***Pax3,*** **a crucial factor for hypaxial muscle differentiation, is regulated by both Mesp2 and Paraxis in the anteriormost PSM and nascent somite region. The present data strongly suggest that patterning events by bHLH-type transcription factors have deep impacts on regional chondrogenic and myogenic differentiation of somitic cells, mainly by means of control of** ***Pax*** **genes.** ***Developmental Dynamics 236:1484–1494, 2007.*** **© 2007 Wiley-Liss, Inc.**

Key words: somitogenesis; sclerotome; vertebra; bHLH factor; Pax genes

Accepted 30 March 2007

INTRODUCTION

Somitogenesis consists of several steps involved in the generation and segmentation of paraxial mesoderm, followed by cellular differentiation, depending on the position of cells within somites (Pourquie, 2003). Before segmental border formation, the presomitic mesoderm derived from primitive steak or tail bud region acquires their periodicity and rostocaudal polarity as a future somite compartment. After segmental border formation and epithelialization, cells located in the dorsal region start to differentiate to dermatomal and myotomal lineages, while cells in ventromedial region de-epithelialize and take on a sclerotomal cell fate for the future axial skeleton. These morphogenetic changes are accompanied with the sequential expression of a great number of genes. Roles of these genes have been revealed by studies in mouse, chick, and zebrafish embryos, by using molecular genetic and experimental embryological techniques.

Mesp1 and *Mesp2* are members of the Mesp family, a group of basic helix–loop–helix (bHLH) transcription

[1]Cellular & Molecular Toxicology Division, National Institute of Health Sciences, Setagayaku, Tokyo
[2]Developmental Genetics, Research Center for Allergy and Immunology (RCAI) RIKEN Yokohama Institute, Tsurumi-ku, Yokohama, Japan
[3]School of Life Sciences, Arizona State University, Tempe, Arizona
[4]Division of Mammalian Development, National Institute of Genetics and Department of Genetics, SOKENDAI, Mishima, Japan
Grant sponsor: The Ministry of Education, Culture, Sports, Science and Technology, Japan.
***Correspondence to: Yu Takahashi, Ph.D., Cellular & Molecular Toxicology Division, National Institute of Health Sciences, 1-18-1 Kamiyoga, Setagayaku, Tokyo 158-8501, Japan. E-mail: yutak@nihs.go.jp**

DOI 10.1002/dvdy.21178
Published online 3 May 2007 in Wiley InterScience (www.interscience.wiley.com).

factors, which is expressed in the anterior presomitic mesoderm (PSM) just before somite formation (Saga et al., 1997). While the Mesp1-null mouse shows no phenotype in somitogenesis, the Mesp2-null mouse shows defects in segment border formation and the rostrocaudal patterning of a somite. Our recent genetic analyses have revealed that Mesp2 plays a central role in the activation of rostral genes *Notch2*, *FGFR1*, *Cer1*, *EphA4*, *Tbx18*, and in suppression of caudal genes such as a Notch ligand *Dll1* and the homeobox transcription factor *Uncx4.1* (Takahashi et al., 2000, 2003; Nakajima et al., 2006). As a result, Mesp2 specifies rostral half property at the expense of caudal half property in the somites. So far, the effects of Mesp2 on skeletal development have been attributed to rostrocaudal patterning and not to general chondrogenic, osteogenic, or myogenic differentiation of somitic cells. While spatially disorganized dermomyotomes are formed, all myogenic factors are expressed in the Mesp2-null embryo, indicating that the general myogenic program is unaffected in the absence of *Mesp2* (Saga et al., 1997). However, our chimera analysis strongly suggests that the Mesp family genes are essential for epithelialization of somitic mesodermal cells (Kitajima et al., 2000; Takahashi et al., 2005).

Paraxis is also a member of the bHLH-type family of transcription factors and is expressed in the anterior two thirds of the presomitic mesoderm, throughout the entire forming epithelial somite, and later the epithelial dermomyotome (Burgess et al., 1995; Barnes et al., 1997; Tseng and Jamrich, 2004). The *Paraxis*-null embryo has segmented somites, but the newly formed somites are not fully epithelialized and fail to form a normal epithelial dermomyotome. This results in the abnormal patterning of many paraxial mesoderm-derived tissues, including the chondrocranium, the axial skeleton, and the ribs (Burgess et al., 1996). In addition, defects in the development of somite-derived nonmigratory hypaxial muscles have been reported (Wilson-Rawls et al., 1999). Although the rostrocaudal polarity is generated in the presomitic mesoderm of paraxis-null embryos, the role of *Paraxis* in epithelialization is required for the maintenance of the rostrocaudal polarity of somites and normal resegmentation of the sclerotome (Johnson et al., 2001). However, the genetic interactions between *Paraxis* and other somite-expressed genes, required for the normal formation of the vertebral column, are not well understood.

Because both *Mesp2* and *Paraxis* are members of bHLH-type transcription factors family, their expression domains in the presomitic mesoderm overlap and the functions of both genes are implicated in somite patterning and mesenchymal–epithelial transition, it is very likely that these genes have a cooperative function. To address this question, we have generated *Mesp2/Paraxis* double-knockout mice. The double-knockout mice exhibited a distinct phenotype that was not expected by the parental single-knockout mice. Foremost, axial skeletal components were extremely reduced in the posterior body and only rudimental lamina of neural arches and ribs remained, which is different from the patterning defects exhibited in the single knockouts. We show that this is the result of a loss of cartilage differentiation from sclerotomal cells. In addition, myotomal components are also severely reduced. Consistent with the perinatal phenotype, we found that the expression of Pax family genes were consistently reduced or lost in the double-knockout embryo. Thus, we conclude that *Mesp2* and *Paraxis* may play a cooperative role to initiate differentiation of both myotomal and sclerotomal cells by regulating Pax family genes.

RESULTS

Mesp2 and *Paraxis* Exhibit Strong Genetic Interaction

An initial indication of a genetic interaction between *Mesp2* and *Paraxis* was obtained by the analysis of skeletal specimens of the double-knockout mouse stained for cartilage and bone. The embryonic day (E) 18.5 wild-type control fetus exhibits a metameric pattern of vertebrae (neural arches and vertebral bodies) and ribs throughout the anterior/posterior (A/P) axis of the body (Fig. 1A,E). The E18.5 fetuses of Mesp2 and Paraxis single-knockout mice show their distinct phenotypes in axial skeletal morphology. The Mesp2-null fetus has vertebrae with completely fused pedicles of neural arches (Fig. 1B) and shows a proximal fusion of ribs as previously described (Saga et al., 1997; Takahashi et al., 2000). In a ventral view of the vertebrae, the vertebral bodies are segmented in the Mesp2-null fetus, although the spatial patterning is somewhat disorganized (Fig. 1F). Thus, Mesp2-null fetus exhibit ectopic formation of skeletal elements derived from the caudal-half of somites, but shows no sign of reduction or loss of skeletal elements. In the Paraxis-null fetus, vertebral bodies are not normally formed at the ventral midline and dual ossification centers are observed in the thoracic and anterior lumbar region (Fig. 1G; Burgess et al., 1996). In addition, the cartilaginous precursors of vertebral bodies are not segmented but are fused along the A/P axis (Fig. 1G; Johnson et al., 2001). In the posterior lumbar region, only rudimental cord-like cartilages, widely separated to left and right sides, are seen instead of the vertebral bodies. A rudimental rod-like cartilage is also seen at the midline. The neural arches are segmented but the lower part of the pedicle is occasionally missing (Fig. 1C). This finding indicates that the Paraxis-null fetus cannot complete formation of the vertebral body at the ventral midline, but the neural arches are relatively normal. In the Mesp2/Paraxis double-null fetus, the skeletal defects are much more severe than the Paraxis-null fetus. In the lumbar region, most parts of the neural arches are not formed, except the dorsal cartilaginous elements corresponding to the lamina (Fig. 1D). From a ventral view, it is apparent that the vertebral bodies are spatially disorganized and hypoplastic in the thoracic and anterior lumbar region. In the posterior lumbar region, only a rudimental rod-like cartilage is observed at the midline (Fig. 1H). Thus, the Mesp2/Paraxis double-null fetus shows extensive loss of skeletal elements both in the vertebral body and neural arches not seen in either the Mesp2- or Paraxis-null fetuses.

To trace the origin of the observed skeletal defects, we analyzed early

cartilage formation in E13.5 embryos using Alcian blue staining. We analyzed embryos in the same litter for the comparison. Cartilage formation of all components of the vertebrae and ribs was observed in the wild-type and Mesp2-null embryos, although the rostrocaudal pattern was perturbed in the Mesp2-null embryo (Fig. 1I,J,M,N). In the Paraxis-null embryo, formation of presumptive vertebral bodies was limited to the cervical, thoracic, and anterior lumbar regions (Fig. 1K,O). Cartilage formation of the neural arches was not largely affected in the Paraxis-null embryo. However, in the double-null embryo, cartilaginous precursors of vertebral bodies appeared more hypoplastic (Fig. 1P). In addition, most of the cartilaginous components of the neural arches were absent and only the precursors of laminae were seen (Fig. 1L). The extent of cartilage formation in both the forelimbs and hindlimbs was comparable among these genotypes, indicating that the above skeletal defects are not due to general developmental retardation. Examination of Alcian blue-stained histological sections also confirmed that cartilage formation was greatly reduced both in Paraxis-null and double-null embryos, and cell density appeared to be reduced especially in the double-null embryo (Fig. 4A–D). In summary, the Mesp2/Paraxis double-null mouse exhibits more severe defects in the axial skeleton than either single-null mice.

Mesp2 and Paraxis Do Not Directly Interact With Each Other

Because both Mesp2 and Paraxis belong to bHLH-type transcription factors and their expression in the PSM is overlapping, we examined the possibility that these two factors might form a heterodimer when they coexist. A yeast two-hybrid assay system was used to address this question (Fields and Bartel, 2001). As bHLH transcription factors usually dimerize with each other through the bHLH domain, and Mesp2 exhibits self-transactivation activity when it was used as a bait, only bHLH domains were used for either factors. As shown in Figure 2, neither Paraxis nor Mesp2 form homodimers or heterodimers with each other, but as a control, do generate heterodimers with the ubiquitously expressed E47. Analysis of mutual regulation between these two genes in single-knockout mice revealed that Paraxis expression is not altered in Mesp2-null embryos and Mesp2 expression is also not altered in Paraxis-null embryos (data not shown). Therefore, these two genes may share the same target genes or lie in the same genetic network.

Mesp2 Establishes and Paraxis Maintains Rostrocaudal Polarity of Somites

Mesp2-null mice exhibit a strongly caudalized vertebral morphology, which is characterized by an almost complete fusion of the pedicles of the neural arches (Fig. 1B). However, the Mesp2/Paraxis double-null fetus showed no pedicles at all (Fig. 1D). This phenotype is quite similar to that of Psen1-null fetus, which shows a rostralization of somites (Takahashi et al., 2000). In addition, *Paraxis* is also implicated in maintenance of the rostrocaudal polarity (Johnson et al., 2001). To test the possibility that the somites in the double-null mice might lack the caudal property, we examined the rostrocaudal polarity of somites in Mesp2/Paraxis double-knockout using several molecular markers.

We have previously shown that the expression pattern of a Notch ligand *Dll1* (Bettenhausen et al., 1995) reflects the rostrocaudal polarity of somites (Takahashi et al., 2000) and that stripes of *Dll1* expression in the caudal-half of somites are not formed in Paraxis-null embryos (Johnson et al., 2001; Fig. 3C). In Mesp2-null embryos, strong expression of *Dll1* in the PSM was expanded to the putative somite region and gradually faded away (Fig. 3B). In the Mesp2/Paraxis double-null embryos, *Dll1* expression was expanded but disappeared relatively suddenly in the mature somite region (Fig. 3D). This finding suggests that maintenance of *Dll1* expression in the mature somite region in both wild-type and Mesp2-null embryos requires *Paraxis*.

Uncx4.1 is not only a caudal molecular marker (Mansouri et al., 1997) but is required for the formation of the pedicles of neural arches, proximal ribs, and transverse processes, which are derived from the caudal-half of somites (Leitges et al., 2000; Mansouri et al., 2000). As shown in Figure 3, *Uncx4.1* expression in the caudal-half of somites (Fig. 3E) was expanded in Mesp2-null embryos, and strong expression was retained in the putative somite region over the length of 10 somites (Fig. 3F). Paraxis-null embryos showed a normal stripe pattern of *Uncx4.1* expression, but expression level was significantly lower than that in the wild-type embryo, especially anterior to the fourth to fifth recently formed somite (Fig. 3G). In Mesp2/Paraxis double-null embryos, the *Uncx4.1* expression pattern was uniform, and the expression level was reduced especially in the putative mature somite region (Fig. 3H). These observations suggest that Paraxis has roles in maintenance of caudal half property, and expression of a key gene for skeletal element specification. To trace descendants of Uncx4.1-positive cells, we crossed these mice with

Fig. 1. Mesp2/Paraxis double-null fetuses exhibit unexpected defects in vertebral morphology. **A–P:** Alcian blue/Alizarin red double-stained skeletal specimens at embryonic day (E) 18.5 (A–H) and E13.5 Alcian blue-stained cartilage specimens of lumbar vertebrae (I–P) in fetuses from Mesp2/Paraxis intercross. Left lateral view (A–D,I–L) and ventral view (E–H,M–P) of indicated genotypes. Note that the Mesp2/Paraxis double-null fetus shows extensive loss of pedicles of the neural arches (D,L) and enhancement of defects in vertebral body formation in Paraxis mutants (H,P). lm, lamina; p, pedicle; t, transverse process; o, ossification center in the vertebral body; na, neural arches; vb, vertebral body. The arrowhead indicates the rudimental rod-like cartilage.

Fig. 2. No direct interactions between Mesp2 and Paraxis proteins. Yeast two-hybrid assay to investigate the interaction specificities between basic helix–loop–helix (bHLH) proteins. Five clones of double transfectants harboring pBTM118 variants and pGAD10 variants were assayed to detect of beta-galactosidase activity. **A–E:** The vector combinations are vacant pGAD10, pGAD10-Mesp1, pGAD10-Mesp2, pGAD10-Paraxis, and pGAD10-E47, against pBTM118-E47 (A); pBTM118-Mesp1 (B); pBTM118-Mesp2 (C); pBTM118-Paraxis (D); and original pBTM118 (E). The results demonstrated that Mesp1, Mesp2, and Paraxis do not form heterodimers with each other, and each of them forms a heterodimer only with E47, a ubiquitous partner.

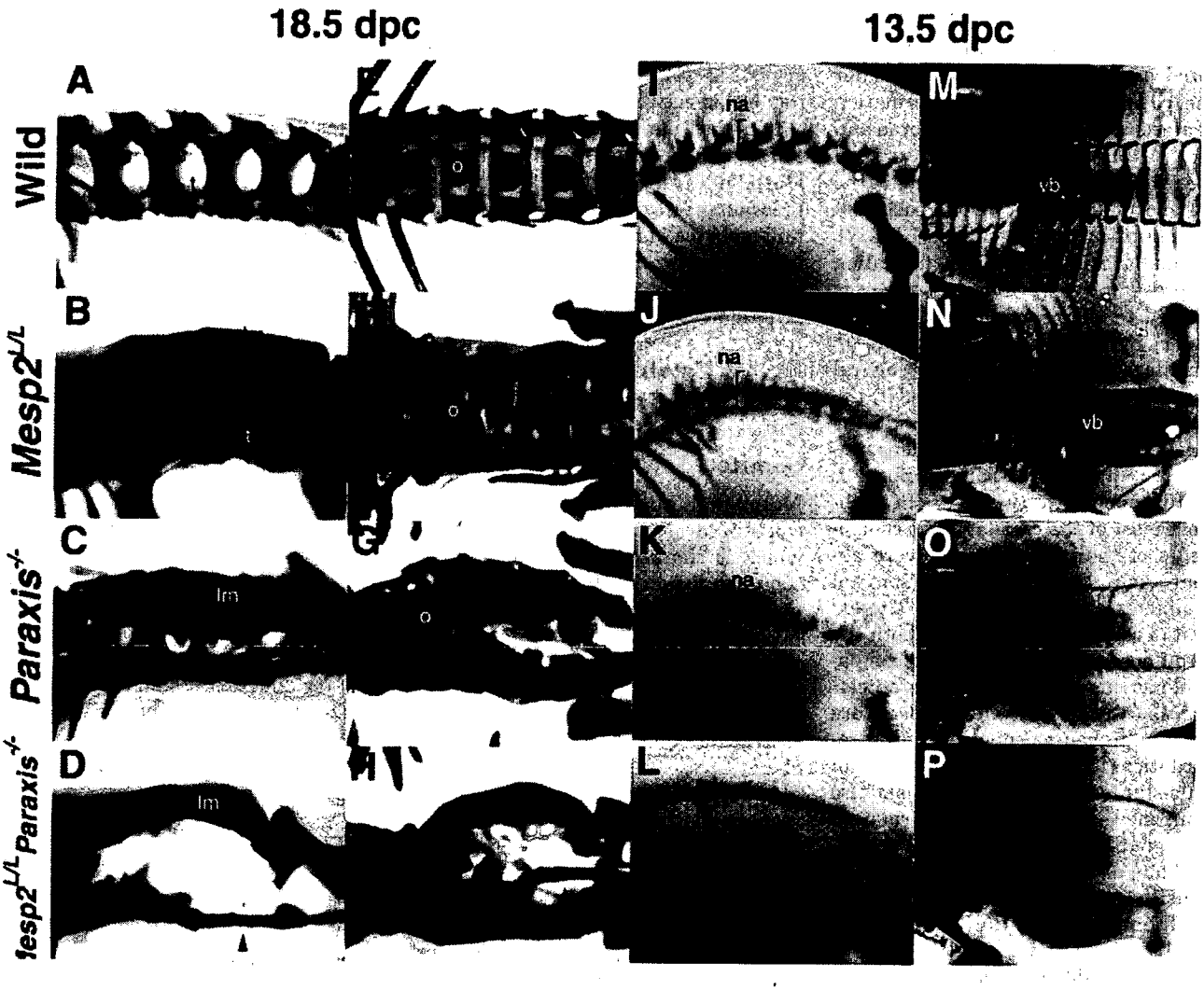

Fig. 1.

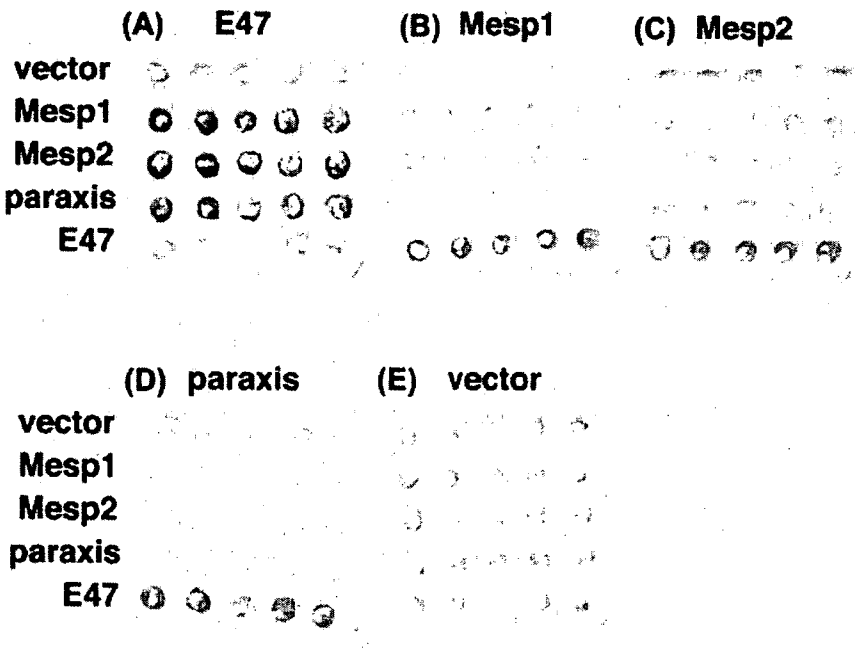

Fig. 2.

Uncx4.1-lacZ transgenic mouse (Fig. 4E–H). As *Uncx4.1* is finally expressed in the caudal lateral sclerotome, the *Uncx4.1-LacZ* mainly labels its derivatives, the pedicle of neural arch, proximal rib, and transverse process. In the lumbar vertebrae of wild-type and Mesp2-null embryos, the pedicle and transverse process were stained (Fig. 4E,F). In Paraxis-null embryos, the transverse process was missing but the pedicle was observed (Fig. 4G). In the Mesp2/Paraxis double-null embryos, staining for neither pedicle nor transverse process was observed (Fig. 4H). Thus, these results confirm observations from the skeletal specimen.

Tbx18 is expressed in the rostral-half of somites and is implicated in the maintenance of the rostral compart-

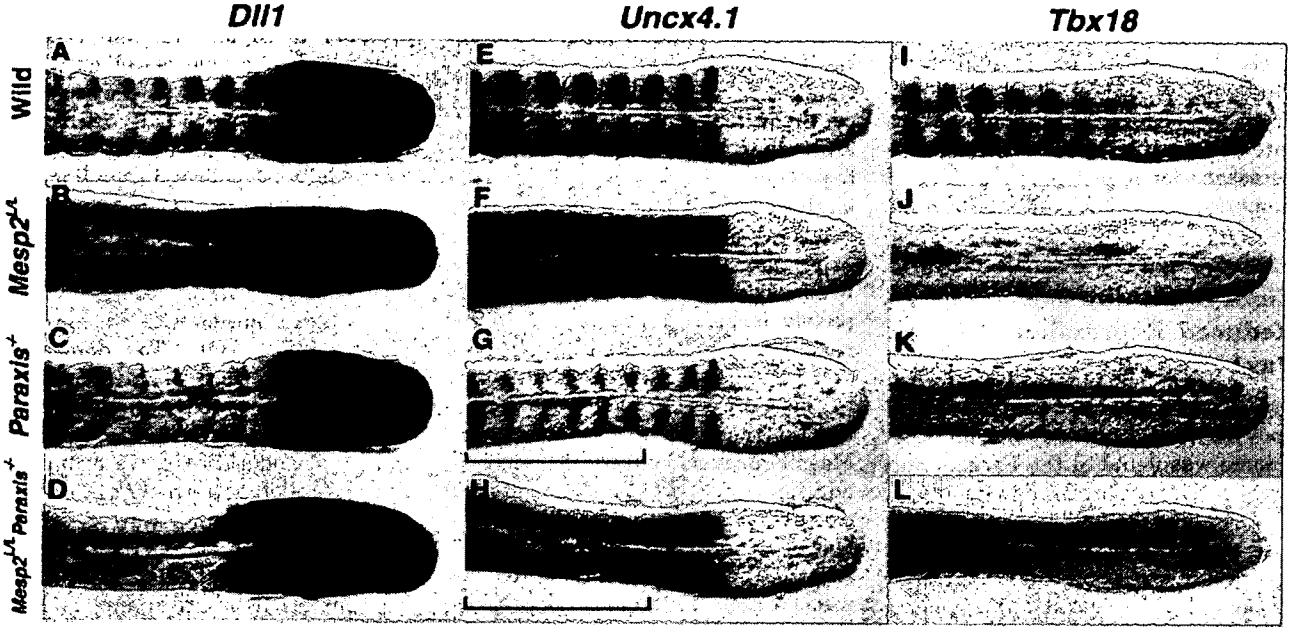

Fig. 3.

Fig. 3. Somites in Mesp2/Paraxis double-null embryos show significant down-regulation of both rostral and caudal gene expression. **A–D:** *Dll1*. **E–H:** *Uncx4.1*. **I–L:** *Tbx18* expression patterns in embryonic day (E) 11.5 embryos with indicated genotypes. While strong expression of *Dll1* and *Uncx4.1* is expanded in Mesp2-null embryos (A,B,E,F), expression of these genes is significantly reduced in both Paraxis-null (C,G) and double-null embryos (D,H), especially in the mature somite region (brackets in G,H). *Tbx18* expression is severely reduced in both Mesp2-null and Paraxis-null, and in double-null embryos (I–L).

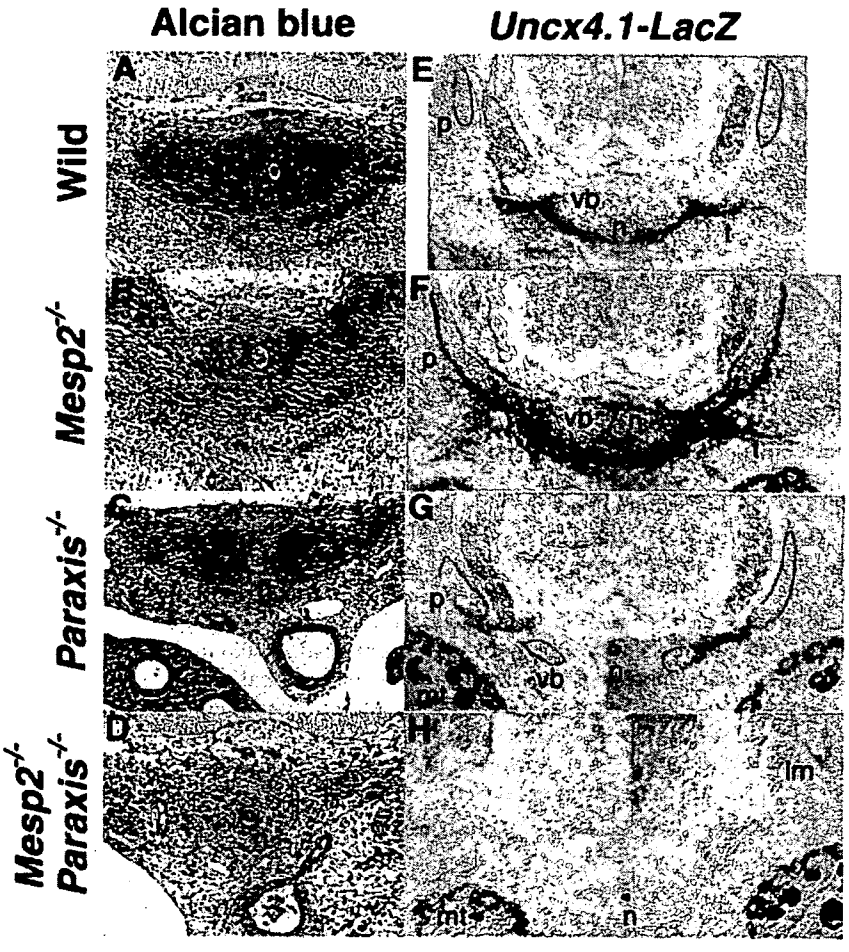

Fig. 4.

Fig. 4. Histological sections confirm the severe defects in vertebral column formation in the Mesp2/Paraxis double-null embryos. **A–H:** Alcian blue-stained (A–D) and X-gal stained (for detection of Uncx4.1-LacZ expressing cells; E–H) transverse sections at the lumbar region at embryonic day (E) 13.5. Note that Paraxis-null fetuses show defects in midline fusion of vertebral body primordia (C,G) and that vertebral column is rudimental in the double-null embryos (D,H). In wild-type and Mesp2-null embryos (E,F), the pedicle (p), transverse process (t), and part of vertebral body (vb) are stained. The staining outlining the notochord of Paraxis-null and Mesp2/Paraxis double-null embryos may represent very rudimental vertebral body as a cord-like structure (Fig. 1, arrowhead). *Uncx4.1* is also expressed in the metanephric mesenchyme, as previously reported (Neidhardt et al., 1997). vb, vertebral body; n, notochord; p, pedicle; t, transverse process; lm, lamina; mt, metanephros.

ment of somites (Bussen et al., 2004). *Tbx18* expression was severely reduced in both Mesp2-null and Paraxis-null, and the double-null embryos (Fig. 3J–L). These results indicate that both Mesp2 and Paraxis are necessary for maintenance of rostral property.

Mesp2/Paraxis Double-Null Embryo Exhibits Severely Reduced Expression of Both Pax1 and Pax9

Significant hypoplasty of the vertebral body derived from the medial sclerotome was found in the Paraxis-null fetus. To understand this phenotype, we examined the differentiation of the medial sclerotome. It is well known that Sonic hedgehog (Shh) expressed in the notochord and floor plate is responsible for both sclerotome induction and survival by means of inducing the target gene Pax1 (Fan and Tessier-Lavigne, 1994; Johnson et al., 1994). The paired box transcription factors Pax1 and Pax9 (Schnittger et al., 1992; Neubuser et al., 1995) are essential for cell proliferation and chondrogenic differentiation of the sclerotome (Wilm et al., 1998; Peters et al., 1999). Other transcription factors expressed in all cartilaginous tissues are Nkx3.2 (Bapx1; Tribioli et al., 1997; Lettice et al., 1999; Tribioli and Lufkin, 1999) and Sox9 (Wright et al., 1995; Bi et al., 1999; Zeng et al., 2002). Bapx1 is known to be a direct target of Pax1 and Pax9 (Rodrigo et al., 2003; see also Fig. 8). In the lumbar region at E11.5, expression of *Pax1*, *Nkx3.1* (not shown), and *Bapx1* in the entire sclerotome and expression of *Sox9* in the ventral sclerotome was severely down-regulated in the Paraxis-null and double-null embryos, indicating that induction of these genes are dependent on Paraxis function (Fig. 5A–D,I–P). The expression pattern of the cartilage-specific marker *Col2a* largely reflected the above expression patterns and results from Alcian blue staining (Fig. 5Q–T). Of interest, these genes did not show abnormal expression in the Mesp2-null embryos. However, a difference between the Paraxis-null and double-null embryos was detected in the expression pattern of another Pax gene, Pax9 (Fig. 5E–H). *Pax9* expression appeared slightly reduced in the Paraxis-null embryo (Fig. 5G), but spatial distribution was normal. In contrast, *Pax9* expression was significantly decreased, especially in the lateral sclerotome in the double-null embryo (Fig. 5H). Whole-mount in situ analysis of E9.5 embryos also confirmed the severe reduction of *Pax9* expression (Fig. 5U–X). Because the Pax1/Pax9 double-null mouse completely lacks vertebral bodies in the vertebrae (Peters et al., 1999), this additional lack of Pax9 may contribute to the more severe defects in formation of the vertebral bodies in the Mesp2/Paraxis double-null fetus. In addition, this severe reduction of *Pax9* expression suggests that the level of *Uncx4.1* expression in the double mutant is functionally insufficient, because a high level of *Pax9* expression in the caudal lateral sclerotome is dependent on Uncx4.1 (Mansouri et al., 2000). Taken together, the observed loss of skeletal elements in the double-null fetus may be attributed to a severe down-regulation of both Pax1 and Pax9 (loss of vertebral body), in addition to dysfunction of Uncx4.1 (loss of pedicles).

Pax3 Expression in the PSM and Nascent Somites Is Regulated by Both Mesp2 and Paraxis

We have also examined expression of several genes involved in myogenesis and tendon formation (Fig. 6). Expression patterns of *myogenin*, *myod* (Sassoon et al., 1989), and *Pax7* (Jostes et al., 1990) in transverse sections at the E11.5 lumbar region revealed that mislocalized myotome formation is seen mainly in Paraxis-null embryos and is further enhanced in the Mesp2/Paraxis double-null embryos. *Scleraxis* expression (Cserjesi et al., 1995; Brent et al., 2003) also confirmed that the normal localization of sclerotome–myotome–syndetome is severely impaired in the double-null embryos (Fig. 6I–L).

Because Paraxis regulates the expression of Pax3 and MyoD, two crucial factors in hypaxial muscle differentiation (Wilson-Rawls et al., 1999), we examined the genetic interactions of Mesp2 and Paraxis on the expression of these genes in the tail somites (Fig. 7). Both epaxial and hypaxial expression of MyoD was observed in Mesp2-null myotome as well as that in wild-type, although MyoD expression was delayed and poor (Fig. 7A,B). Hypaxial myotome formation was delayed and mislocalized in the Paraxis-null embryo (Fig. 7C). The Mesp2/Paraxis double-null embryo shows a more severe reduction in MyoD-expressing cell populations and hypaxial myotome formation was seldom detected (Fig. 7D). To determine whether the defects in myotome formation of the double-null embryo result from an additive effect from a lack of Mesp2 and Paraxis, we examined the expression pattern of *Pax3*, a gene upstream of MyoD (Maroto et al., 1997; Tajbakhsh et al., 1997). In the wild-type embryo, *Pax3* expression was observed in the anteriormost PSM and somites and was localized to the dermomyotome in the mature somites (Fig. 8E; Williams and Ordahl, 1994). In the Mesp2-null embryo, *Pax3* expression in the recently formed somite region was down-regulated, while that in the anteriormost PSM and dermomyotome of the mature somite region was relatively unaffected (Fig. 8F). The Paraxis-null embryo showed severely decreased *Pax3* expression in the dermomyotome, while expression in the anteriormost PSM and forming somites was maintained (Fig. 8G and Wilson-Rawls et al., 1999). Expression of *Pax3* was severely decreased in the Mesp2/Paraxis double-null embryo, resulting in an almost complete loss of Pax3 expression throughout the paraxial mesoderm (Fig. 8H). This finding suggests that Mesp2 and Paraxis cooperatively regulate *Pax3* expression in the anteriormost PSM and forming somites, and that the observed effects on myotome formation are not only additive but also include a synergistic effect on hypaxial myogenesis.

DISCUSSION

Paraxis is a bHLH transcription factor expressed in the anterior PSM, entire somite, and then dermomyotomal compartment of mature somites in mouse and chick embryos, and is implicated in multiple aspects of somitogenesis. Although its roles in epithelialization of somites (Burgess et al.,

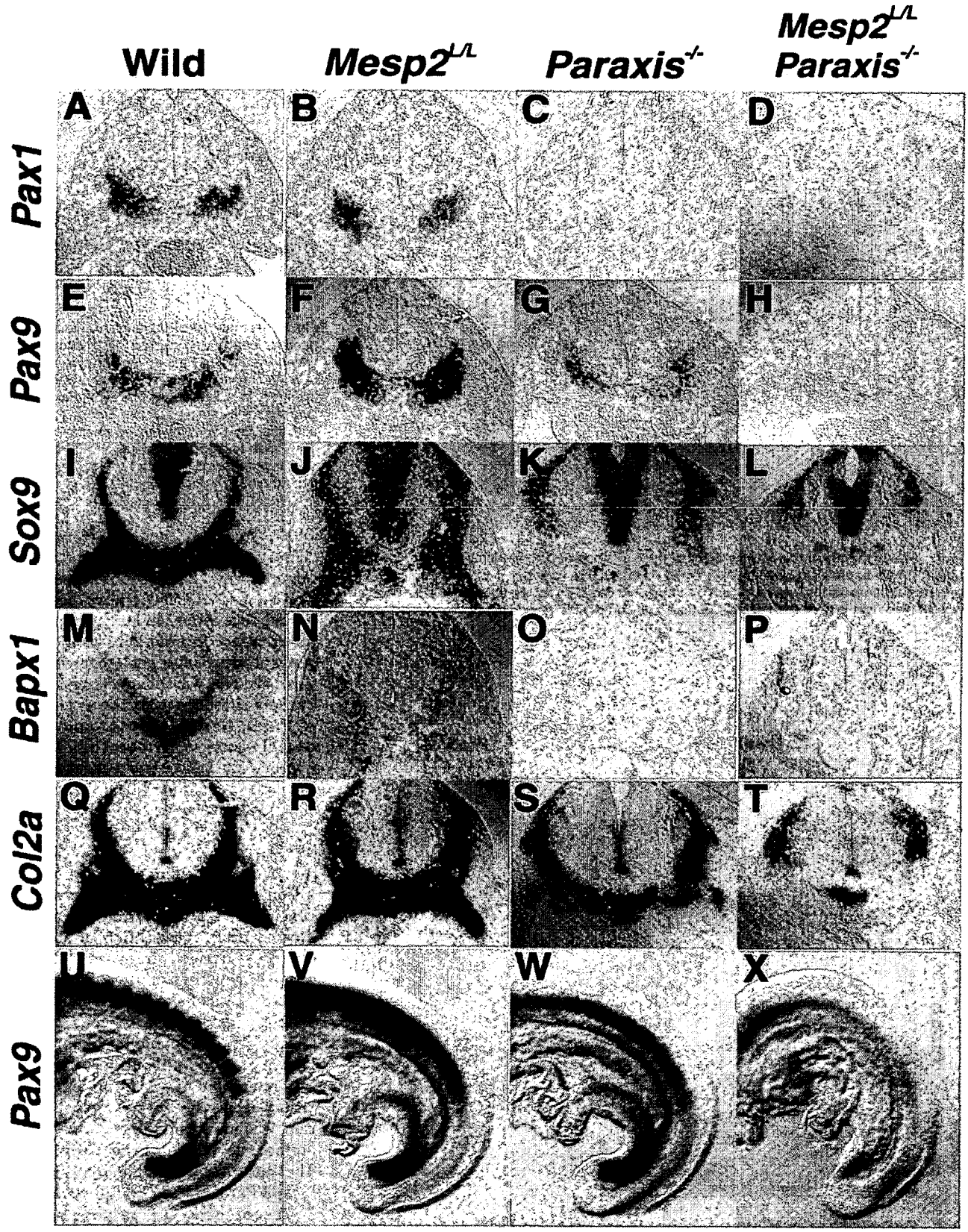

Fig. 5. Analysis of sclerotomal and chondrogenic gene expression in the Mesp2/Paraxis double-null embryos. **A–T:** Expression of *Pax1* (A–D), *Pax9* (E–H), *Sox9* (I–L), *Bapx1* (M–P), and *Col2a* (Q–T) in transverse sections at the lumbar region at embryonic day (E) 11.5. Note that *Pax1*, *Sox9*, and *Bapx1* expression is reduced in the absence of Paraxis, and *Pax9* expression is severely decreased in the double mutant. **U–X:** Whole-mount specimen at E9.5 confirms the severe reduction of *Pax9* expression.

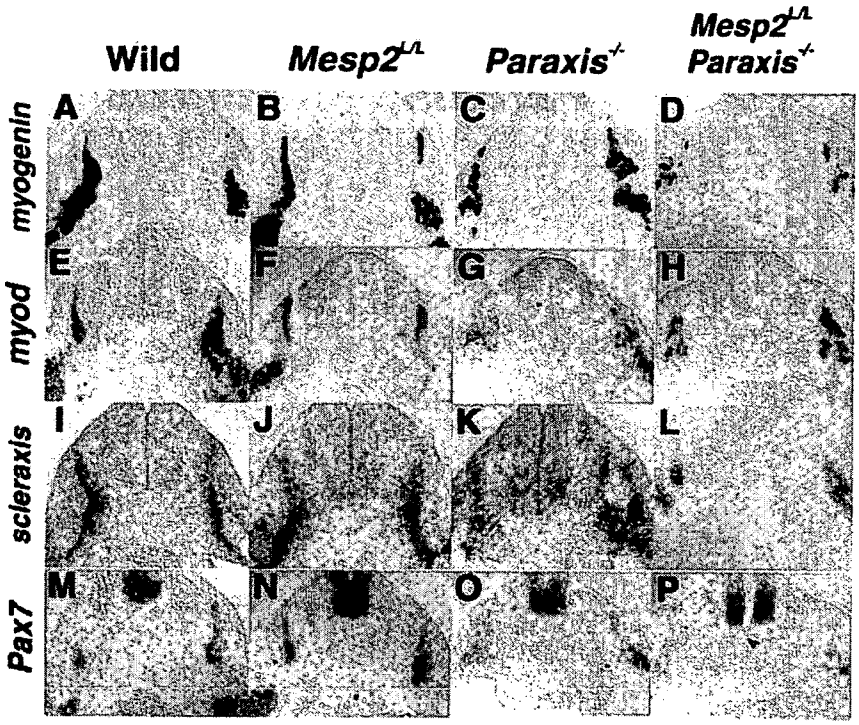

Fig. 6. Analysis of myotomal and syndetomal gene expression in the Mesp2/Paraxis double-null embryos. **A–P:** Expression of *myogenin* (A–D), *myod* (E–H), *scleraxis* (I–L), and *Pax7* (M–P) in transverse sections at the lumbar region at embryonic day (E) 11.5. Note that the spatial organization of myotome is perturbed in both Paraxis-null and double-null embryos.

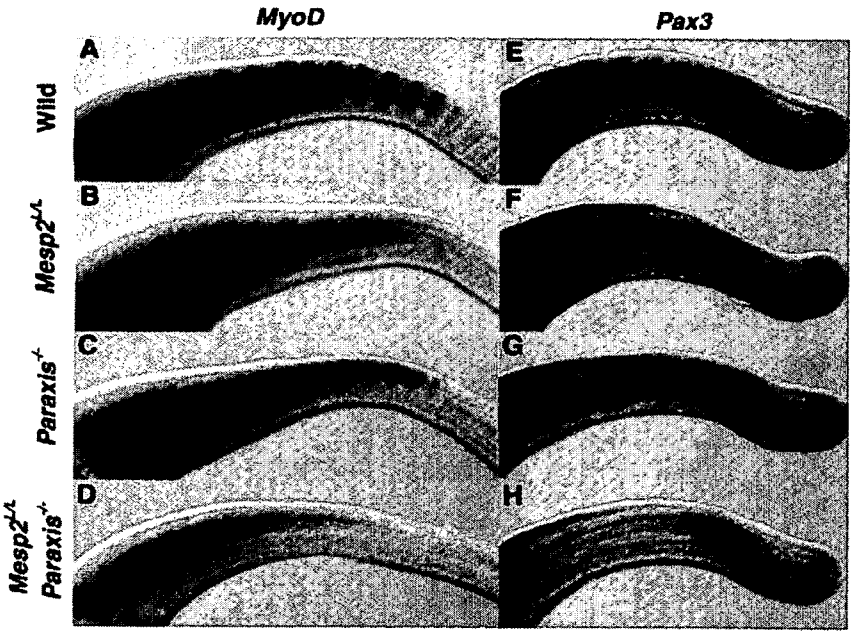

Fig. 7. *Pax3* expression in the nascent somite region is regulated by both Mesp2 and Paraxis. **A–H:** *Myod* (A–D) and *Pax3* (E–H) expression of embryonic day (E) 11.5 in the tail region. Note that *myod* expression appears delayed and severely disrupted (D), and *Pax3* expression in the nascent somite region is severely reduced (H) in the double-null embryo.

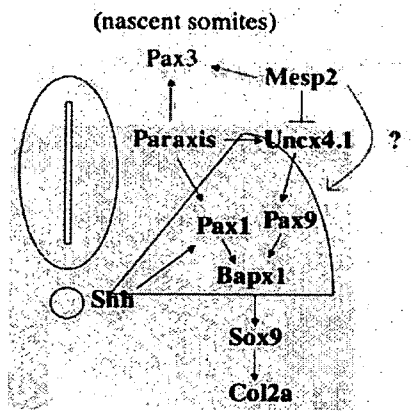

Fig. 8. A schematic illustration for the putative genetic network, including interactions between Mesp2 and Paraxis. Red arrows indicate new findings in the current study. Paraxis is involved in expression of both Pax1 and Uncx4.1. Mesp2 suppresses Uncx4.1, which activates Pax9, but might also positively regulate Pax9. In addition, Mesp2 and Paraxis redundantly regulate Pax3 expression in the nascent somites.

1996), hypaxial myotome formation (Wilson-Rawls et al., 1999) and maintenance of rostrocaudal polarity (Johnson et al., 2001) have been reported, less attention has been paid to its genetic interaction with other genes during axial skeletogenesis. In this study, we have shown that Paraxis is required for the expression of Pax1, Nkx3.1, Bapx1, and Sox9, crucial factors in vertebral column formation, in the ventral sclerotome in the posterior body. These findings suggest that *Paraxis* has significant roles in formation of the vertebral body at the ventral midline. Mesp2-null fetuses exhibit almost complete fusion of neural arches and proximal rib elements, and this defect is attributed to ectopic formation of skeletal elements derived from caudal half compartment of somites. So far, no sign of a loss of skeletal elements has been suggested from previous genetic analyses using double-knockout studies with Mesp2-null mice. Therefore, the reduction of vertebral elements observed in the Mesp2/Paraxis mutant was surprising and led us to examine the caudal gene expression. The most striking phenotype in the Mesp2/Paraxis double-null vertebrae is the extensive loss of pedicles. We have found that expression level of *Uncx4.1* is significantly reduced in both Paraxis-null and Mesp2/Paraxis

double-null embryos, especially in the mature somite region. The reduction of *Uncx4.1* expression in the Paraxis-null embryo may contribute to the partial loss of the pedicles and loss of proximal portion of ribs. Although the low level of *Uncx4.1* stripe expression in Paraxis-null embryo is sufficient for formation of pedicles, the diffuse and low expression of *Uncx4.1* in the Mesp2/Paraxis double-null embryo may be insufficient for formation of pedicles. Because *Pax1* expression was severely reduced in the Paraxis-null mutant, we initially asked whether the lack of Pax1 and the additional loss of Mesp2 might be responsible for the compromised sclerotomal program by generating Mesp2/Pax1 double-null mice. These compound-null mice, however, exhibited only additive skeletal phenotype and did not show the loss of vertebral bodies and pedicles observed in the Mesp2/Paraxis double-mutants (data not shown). Our further analysis of sclerotomal gene expression clarified that, in addition to *Pax1*, *Pax9* expression is significantly down-regulated in the Mesp2/Paraxis double-null embryo. Because Pax1/Pax9 double-null mouse completely lacks vertebral bodies in the vertebrae (Peters et al., 1999), this additional lack of Pax9 may contribute to the severer defects in formation of the vertebral bodies in the Mesp2/Paraxis double-null fetus (Fig. 8).

The extent of reduction of *Pax9* appears much more severe than that of *Uncx4.1* in the double mutants. Although *Pax1* and *Pax9* are initially expressed in the entire sclerotome, later *Pax1* becomes predominantly expressed in the ventromedial sclerotome and *Pax9* expression becomes stronger in the ventrolateral sclerotome, suggesting some differential usage of the two genes. In addition, strong *Pax9* expression in the caudal lateral sclerotome is dependent on Uncx4.1, suggesting its involvement in pedicle formation (Mansouri et al., 2000; Fig. 8). Thus, in the absence of Uncx4.1, the potential functions of Pax9 are also lost. It is noted that, in the Pax1/Pax9 double-null embryos, the proximal parts of ribs are missing in addition to the vertebral bodies and intervertebral discs (Peters et al., 1999), suggesting roles of Pax9 in the lateral sclerotome. In the nascent somite, Mesp2 suppresses *Uncx4.1*, which activates *Pax9*, and thus *Uncx4.1* and *Pax9* expression is stronger in the Mesp2-null condition. In the absence of Paraxis, however, this up-regulation of *Uncx4.1* does not occur and additional loss of Mesp2 causes down-regulation of *Pax9*. Therefore, Mesp2 may positively regulate *Pax9* independently of Uncx4.1 (Fig. 8).

Mesp2 is necessary for the normal spatial patterning of the myotome (Saga et al., 1997). Mesp2-null embryos show significant delay and perturbation of myogenesis (Fig. 7), and the current study has revealed that *Pax3* expression is regulated by both Paraxis and Mesp2 in the anterior-most PSM and nascent somite region. As the *Pax3* expression domain overlaps with those of *Paraxis* and *Mesp2* at this region, it is possible that these two factors directly regulate the *Pax3* gene. *Pax9* appears to be expressed in the formed somites, after robust Mesp2 expression ceases, suggesting indirect regulation. The current study has revealed previously unrecognized interactions between Mesp2 and Paraxis in the formation of axial skeleton and musculature. Analysis of molecular interactions between these factors and Pax genes, as well as Uncx4.1, will contribute to understanding of genetic network underlying somitogenesis.

EXPERIMENTAL PROCEDURES

Animals

The *Paraxis*-null mice (Burgess et al., 1996) and *Mesp2-LacZ* knockin mice (Takahashi et al., 2000) were maintained as heterozygotes with an ICR background in the National Institute of Health Sciences, Tokyo. The double heterozygous mice were mated to obtain the Mesp2/Paraxis double-null embryos. The *Mesp2-LacZ* knockin mice has impaired Mesp1 function in addition to lack of Mesp2, thus were suitable for analyzing roles of the Mesp family in somitogenesis (Morimoto et al., 2006).

Yeast Two Hybrid Assay

A cDNA fragment of *Mesp2* encoding a bHLH domain (from Q80 to L139 in MESP2) was fused in-frame to the *lexA*-coding sequence in vector pBTM118 (Fields and Bartel, 2001). The L40, a yeast strain containing *lexA-HIS3* and *lexA-lacZ* reporter genes, was first transformed with pBTM118-*Mesp2*, and then with a mouse E11 cDNA library constructed in pGAD10 (Gal4 activation domain fusion vector, Clontech), using the lithium acetate method. Six hundred independent colonies were isolated from 1 × 106 transformants on the selective media plate lacking leucine, tryptophan, and histidine and supplemented with 5 mM 3-aminotriazole. All these clones were restreaked onto the selection medium and assayed for beta-galactosidase activity by a filter assay (Vojtek et al., 1993). The plasmids containing cDNA fragments were isolated from yeast culture, and the cDNAs were characterized by sequencing analysis and similarity search using NCBI programs (BLASTn). We identified E47 as an interacter for Mesp2.

To test for interaction specificity, we constructed the pBTM118 and pGAD10 variants expressing fusion proteins of Mesp1, Mesp2, and Paraxis and E47. Although full-length cDNAs were inserted into pGAD10, the fragmental cDNAs including a bHLH domain were used to construct pBTM118 variants, because the full-length cDNAs exhibited cognate activity of Gal4. cDNA fragments coding for Mesp1 (G74 to S137), Mesp2 (Q80 to L139), Paraxis (R67 to L126), and E47 (410A to 650G) were inserted. Then, the resulting pBTM118 and pGAD10 variants were cotransfected into L40 and selected on the selective media plate supplemented with histidine. Aroused colonies were restreaked on the same plate and used for a filter assay to detect beta-galactosidase activity.

In Situ Hybridization, Histological Analysis, and Skeletal Preparations

The methods used for whole-mount and section in situ hybridization, histology, and skeletal preparation by Al-

cian blue/Alizarin red staining are as described in our previous reports (Saga et al., 1997; Takahashi et al., 2000). For Alcian blue staining of paraffin sections, deparaffinized and rehydrated sections were treated with 3% acetic acid for 2 min, and then stained with 1% Alcian blue/3% acetic acid for 30 min. For detection of beta-galactosidase activity in *Uncx-LacZ*–expressing cells, embryos were fixed in 2% paraformaldehyde, 0.2% glutaraldehyde, and 0.02% NP-40 in phosphate buffered saline for 30–60 min at room temperature. After embedded in OCT compound, frozen sections were cut at 8 μm, dried overnight, and stained with X-gal solution for several hours. The sections were briefly counterstained with eosin.

ACKNOWLEDGMENTS

We thank Randy Johnson for providing us the Uncx4.1-LacZ transgenic mouse line and the following researchers for cDNA clones encoding *Dll1* (A. Gossler), *Uncx4.1*, *Pax7* (P. Gruss), *Sox9*, and *Col2a* (K.S.E. Cheah). We also thank M. Ikumi, C. Fujihira, and E. Ikeno for technical assistance and Douglas Anderson for editorial assistance. This work was supported by Grants-in-Aid for Science Research on Priority Areas (B), the Organized Research Combination System, and National BioResource Project of the Ministry of Education, Culture, Sports, Science and Technology, Japan.

REFERENCES

Barnes GL, Alexander PG, Hsu CW, Mariani BD, Tuan RS. 1997. Cloning and characterization of chicken Paraxis: a regulator of paraxial mesoderm development and somite formation. Dev Biol 189: 95–111.

Bettenhausen B, Hrabe de Angelis M, Simon D, Guenet JL, Gossler A. 1995. Transient and restricted expression during mouse embryogenesis of Dll1, a murine gene closely related to Drosophila Delta. Development 121:2407–2418.

Bi W, Deng JM, Zhang Z, Behringer RR, de Crombrugghe B. 1999. Sox9 is required for cartilage formation. Nat Genet 22:85–89.

Brent AE, Schweitzer R, Tabin CJ. 2003. A somitic compartment of tendon progenitors. Cell 113:235–248.

Burgess R, Cserjesi P, Ligon KL, Olson EN. 1995. Paraxis: a basic helix-loop-helix protein expressed in paraxial mesoderm and developing somites. Dev Biol 168:296–306.

Burgess R, Rawls A, Brown D, Bradley A, Olson EN. 1996. Requirement of the paraxis gene for somite formation and musculoskeletal patterning. Nature 384: 570–573.

Bussen M, Petry M, Schuster-Gossler K, Leitges M, Gossler A, Kispert A. 2004. The T-box transcription factor Tbx18 maintains the separation of anterior and posterior somite compartments. Genes Dev 18:1209–1221.

Cserjesi P, Brown D, Ligon KL, Lyons GE, Copeland NG, Gilbert DJ, Jenkins NA, Olson EN. 1995. Scleraxis: a basic helix-loop-helix protein that prefigures skeletal formation during mouse embryogenesis. Development 121:1099–1110.

Fan CM, Tessier-Lavigne M. 1994. Patterning of mammalian somites by surface ectoderm and notochord: evidence for sclerotome induction by a hedgehog homolog. Cell 79:1175–1186.

Fields S, Bartel PL. 2001. The two-hybrid system. A personal view. Methods Mol Biol 177:3–8.

Johnson RL, Laufer E, Riddle RD, Tabin C. 1994. Ectopic expression of Sonic hedgehog alters dorsal-ventral patterning of somites. Cell 79:1165–1173.

Johnson J, Rhee J, Parsons SM, Brown D, Olson EN, Rawls A. 2001. The anterior/posterior polarity of somites is disrupted in paraxis-deficient mice. Dev Biol 229: 176–187.

Jostes B, Walther C, Gruss P. 1990. The murine paired box gene, Pax7, is expressed specifically during the development of the nervous and muscular system. Mech Dev 33:27–37.

Kitajima S, Takagi A, Inoue T, Saga Y. 2000. MesP1 and MesP2 are essential for the development of cardiac mesoderm. Development 127:3215–3226.

Leitges M, Neidhardt L, Haenig B, Herrmann BG, Kispert A. 2000. The paired homeobox gene Uncx4.1 specifies pedicles, transverse processes and proximal ribs of the vertebral column. Development 127:2259–2267.

Lettice LA, Purdie LA, Carlson GJ, Kilanowski F, Dorin J, Hill RE. 1999. The mouse bagpipe gene controls development of axial skeleton, skull, and spleen. Proc Natl Acad Sci U S A 96:9695–9700.

Mansouri A, Yokota Y, Wehr R, Copeland NG, Jenkins NA, Gruss P. 1997. Paired-related murine homeobox gene expressed in the developing sclerotome, kidney, and nervous system. Dev Dyn 210:53–65.

Mansouri A, Voss AK, Thomas T, Yokota Y, Gruss P. 2000. Uncx4.1 is required for the formation of the pedicles and proximal ribs and acts upstream of Pax9. Development 127:2251–2258.

Maroto M, Reshef R, Munsterberg AE, Koester S, Goulding M, Lassar AB. 1997. Ectopic Pax-3 activates MyoD and Myf-5 expression in embryonic mesoderm and neural tissue. Cell 89:139–148.

Morimoto M, Kiso M, Sasaki N, Saga Y. 2006. Cooperative Mesp activity is required for normal somitogenesis along the anterior-posterior axis. Dev Biol 300: 687–698.

Nakajima Y, Morimoto M, Takahashi Y, Koseki H, Saga Y. 2006. Identification of Epha4 enhancer required for segmental expression and the regulation by Mesp2. Development 133:2517–2525.

Neidhardt LM, Kispert A, Herrmann BG. 1997. A mouse gene of the paired-related homeobox class expressed in the caudal somite compartment and in the developing vertebral column, kidney and nervous system. Dev Genes Evol 207:330–339.

Neubuser A, Koseki H, Balling R. 1995. Characterization and developmental expression of Pax9, a paired-box-containing gene related to Pax1. Dev Biol 170: 701–716.

Peters H, Wilm B, Sakai N, Imai K, Maas R, Balling R. 1999. Pax1 and Pax9 synergistically regulate vertebral column development. Development 126:5399–5408.

Pourquie O. 2003. Vertebrate somitogenesis: a novel paradigm for animal segmentation? Int J Dev Biol 47:597–603.

Rodrigo I, Hill RE, Balling R, Munsterberg A, Imai K. 2003. Pax1 and Pax9 activate Bapx1 to induce chondrogenic differentiation in the sclerotome. Development 130: 473–482.

Saga Y, Hata N, Koseki H, Taketo MM. 1997. Mesp2: a novel mouse gene expressed in the presegmented mesoderm and essential for segmentation initiation. Genes Dev 11:1827–1839.

Sassoon D, Lyons G, Wright WE, Lin V, Lassar A, Weintraub H, Buckingham M. 1989. Expression of two myogenic regulatory factors myogenin and MyoD1 during mouse embryogenesis. Nature 341: 303–307.

Schnittger S, Rao VV, Deutsch U, Gruss P, Balling R, Hansmann I. 1992. Pax1, a member of the paired box-containing class of developmental control genes, is mapped to human chromosome 20p11.2 by in situ hybridization (ISH and FISH). Genomics 14:740–744.

Tajbakhsh S, Rocancourt D, Cossu G, Buckingham M. 1997. Redefining the genetic hierarchies controlling skeletal myogenesis: Pax-3 and Myf-5 act upstream of MyoD. Cell 89:127–138.

Takahashi Y, Koizumi K, Takagi A, Kitajima S, Inoue T, Koseki H, Saga Y. 2000. Mesp2 initiates somite segmentation through the Notch signalling pathway. Nat Genet 25:390–396.

Takahashi Y, Inoue T, Gossler A, Saga Y. 2003. Feedback loops comprising Dll1, Dll3 and Mesp2, and differential involvement of Psen1 are essential for rostrocaudal patterning of somites. Development 130:4259–4268.

Takahashi Y, Kitajima S, Inoue T, Kanno J, Saga Y. 2005. Differential contributions of Mesp1 and Mesp2 to the epithelialization and rostro-caudal patterning of somites. Development 132:787–796.

Tribioli C, Lufkin T. 1999. The murine Bapx1 homeobox gene plays a critical role in embryonic development of the ax-

ial skeleton and spleen. Development 126: 5699–5711.
Tribioli C, Frasch M, Lufkin T. 1997. Bapx1: an evolutionary conserved homologue of the Drosophila bagpipe homeobox gene is expressed in splanchnic mesoderm and the embryonic skeleton. Mech Dev 65:145–162.
Tseng HT, Jamrich M. 2004. Identification and developmental expression of Xenopus paraxis. Int J Dev Biol 48:1155–1158.
Vojtek AB, Hollenberg SM, Cooper JA. 1993. Mammalian Ras interacts directly with the serine/threonine kinase Raf. Cell 74:205–214.
Williams BA, Ordahl CP. 1994. Pax-3 expression in segmental mesoderm marks early stages in myogenic cell specification. Development 120:785–796.
Wilm B, Dahl E, Peters H, Balling R, Imai K. 1998. Targeted disruption of Pax1 defines its null phenotype and proves haploinsufficiency. Proc Natl Acad Sci U S A 95:8692–8697.
Wilson-Rawls J, Hurt CR, Parsons SM, Rawls A. 1999. Differential regulation of epaxial and hypaxial muscle development by paraxis. Development 126:5217–5229.
Wright E, Hargrave MR, Christiansen J, Cooper L, Kun J, Evans T, Gangadharan U, Greenfield A, Koopman P. 1995. The Sry-related gene Sox9 is expressed during chondrogenesis in mouse embryos. Nat Genet 9:15–20.
Zeng L, Kempf H, Murtaugh LC, Sato ME, Lassar AB. 2002. Shh establishes an Nkx3.2/Sox9 autoregulatory loop that is maintained by BMP signals to induce somitic chondrogenesis. Genes Dev 16: 1990–2005.

nature immunology

The adaptor protein CARD9 is essential for the activation of myeloid cells through ITAM-associated and Toll-like receptors

Hiromitsu Hara[1,2], Chitose Ishihara[1], Arata Takeuchi[1], Takayuki Imanishi[1], Liquan Xue[3], Stephan W Morris[3], Masanori Inui[4], Toshiyuki Takai[4], Akira Shibuya[5], Shinobu Saijo[6], Yoichiro Iwakura[6], Naohito Ohno[7], Haruhiko Koseki[8], Hiroki Yoshida[2], Josef M Penninger[9] & Takashi Saito[1]

Immunoreceptor tyrosine-based activation motifs (ITAMs) are crucial in antigen receptor signaling in acquired immunity. Although receptors associated with the ITAM-bearing adaptors FcRγ and DAP12 on myeloid cells have been suggested to activate innate immune responses, the mechanism coupling those receptors to 'downstream' signaling events is unclear. The CARMA1–Bcl-10–MALT1 complex is critical for the activation of transcription factor NF-κB in lymphocytes but has an unclear function in myeloid cells. Here we report that deletion of the gene encoding the Bcl-10 adaptor–binding partner CARD9 resulted in impaired myeloid cell activation of NF-κB signaling by several ITAM-associated receptors. Moreover, CARD9 was required for Toll-like receptor–induced activation of dendritic cells through the activation of mitogen-activated protein kinases. Although *Bcl10*$^{-/-}$ and *Card9*$^{-/-}$ mice had similar signaling impairment in myeloid cells, *Card11*$^{-/-}$ (CARMA1-deficient) myeloid cell responses were normal, and although *Card11*$^{-/-}$ lymphocytes were defective in antigen receptor–mediated activation, *Card9*$^{-/-}$ lymphocytes were not. Thus, the activation of lymphoid and myeloid cells through ITAM-associated receptors or Toll-like receptors is regulated by CARMA1–Bcl-10 and CARD9–Bcl-10, respectively.

T cells and B cells, which are mainly responsible for regulating acquired immunity, are activated through T cell receptors (TCRs) and B cell receptors (BCRs). Those antigen receptors 'trigger' activation signals by associating with signaling molecules such as CD3 proteins or immunoglobulin-α (Igα) and Igβ, which contain immunoreceptor tyrosine-based activation motifs (ITAMs) in their cytoplasmic domains[1]. The activation signal is transduced by the phosphorylation of specific tyrosine residues in the ITAMs and subsequent recruitment of the tyrosine kinases Syk or Zap70 to the phosphorylated ITAMs. In addition to lymphocytes, natural killer cells and myeloid lineage cells such as mast cells, macrophages, neutrophils and dendritic cells (DCs)[2] also express receptors that transduce their signals through ITAMs and regulate cell functions in innate immunity.

Two ITAM-containing adaptor proteins, DAP12 and FcRγ, are known to associate with receptors in myeloid cells (ITAM-associated receptors); for the myeloid receptors, signaling from the receptor is mediated by the ITAM-containing adaptors and subsequently leads to Syk activation. FcRγ is required for the activation of Fc receptors on myeloid cells, including FcγRI (CD64) and FcγRIII (CD16) for IgG, and FcεRI for IgE. Other FcRγ-associated activation receptors expressed on myeloid cells include PIR-A[3,4], LIR[5], DCAR[6] and OSCAR[7]. DAP12-associated myeloid receptors include the TREM family of receptors[8], MDL-1 (ref. 9), SIRP-β[10], PILRβ[11], IREM2 (ref. 12), CD200R[13] and MAIR-II (LMIR-2)[14].

Stimulation of those FcRγ- or DAP12-associated receptors on myeloid cells induces various signaling pathways leading to the production of cytokines and/or chemokines. FcγRI- and FcγRIII-mediated activation of macrophages triggers the generation of inflammatory cytokines and reactive oxygen species[15]. OSCAR stimulation leads to cytokine release and DC survival through the activation of pathways dependent on the kinase Erk and phosphatidylinositol-3-OH kinase[16]. Ligation of TREM-1 induces the production of inflammatory chemokines and cytokines such as interleukin 8 (IL-8) and myeloperoxidase in neutrophils and monocytes as well as the

[1]Laboratory for Cell Signaling, RIKEN Research Center for Allergy and Immunology, Yokohama, Kanagawa 230-0045, Japan. [2]Department of Biomolecular Sciences, Faculty of Medicine, Saga University, Saga, Saga 849-8501, Japan. [3]Department of Pathology and Oncology, St. Jude Children's Research Hospital, Memphis, Tennessee 38105, USA. [4]Department of Experimental Immunology, Institute of Development, Aging and Cancer, Tohoku University, Sendai, Miyagi 980-8575, Japan. [5]Department of Immunology, Institute of Basic Medical Sciences, University of Tsukuba, Tsukuba, Ibaraki 305-8575, Japan. [6]Center for Experimental Medicine, The Institute of Medical Science, The University of Tokyo, Minato-ku, Tokyo 108-8639, Japan. [7]Laboratory for Immunopharmacology of Microbial Products, School of Pharmacy, Tokyo University of Pharmacy and Life Science, Hachioji, Tokyo 192-0392, Japan. [8]Laboratory for Developmental Genetics, RIKEN Research Center for Allergy and Immunology, Yokohama, Kanagawa 230-0045, Japan. [9]Institute of Molecular Biotechnology of the Austrian Academy of Sciences, 1030 Vienna, Austria. Correspondence should be addressed to T.S. (saito@rcai.riken.jp) or H.H. (harah@cc.saga-u.ac.jp).

Received 23 January; accepted 13 April; published online 7 May 2007; doi:10.1038/ni1466

production of chemotactic protein 1 and tumor necrosis factor (TNF) in monocytes[17]. Studies demonstrating that treatment of mice with a soluble TREM-1–Ig fusion protein can prevent death by lipopolysaccharide (LPS)–induced septic shock suggest involvement of TREM-1 in amplifying LPS signals[18]. Triggering MAIR-II also induces the secretion of proinflammatory cytokines and/or chemokines from macrophages[14]. Moreover, ITAM-associated receptor–mediated stimulation has been also shown to induce DC maturation[16,17]. Thus, signals through the ITAM-associated receptors mediate the activation and maturation of macrophages and DCs. However, the molecular mechanisms underlying the coupling of the ITAM-associated receptor triggering to the induction of inflammatory gene expression have remained poorly understood.

In addition to the ITAM-associated receptors discussed above, myeloid cells express DC-associated C-type lectin 1 (dectin-1), which contains an atypical ITAM in its cytoplasmic tail[19]. Unlike typical ITAMs, which require two phosphorylated tyrosine residues in the motif for Syk recruitment, only one tyrosine is required for the recruitment of Syk to the dectin-1 atypical ITAM. Dectin-1 is a pattern-recognition receptor for β-glucan mainly present in the fungal cell wall. Zymosan, a yeast cell wall extract composed mainly of β-glucan and other various components, can stimulate dectin-1 to produce inflammatory cytokines such as IL-2, TNF, IL-6, IL-10 and IL-12. It has been shown that zymosan can also stimulate Toll-like receptor 2 (TLR2) to produce certain cytokines such as TNF and IL-12 through the activation of NF-κB mediated by the adaptor protein MyD88 (myeloid differentiation primary-response gene 88)[20]. It has been suggested that dectin-1 induces both Syk-dependent and Syk-independent signaling pathways in macrophages and DCs. Although cooperative signaling is required with TLR2, dectin-1-induced production of IL-12 and TNF is Syk independent, whereas IL-2 and IL-10 production is Syk dependent[21]. However, how dectin-1-mediated signals integrate with TLR signals and the mechanism by which the Syk-dependent and Syk-independent pathways are regulated to trigger different sets of cytokine genes are unknown.

The caspase-recruitment domain (CARD) is a protein-binding module that mediates the assembly of CARD-containing proteins. One of the CARD proteins, Bcl-10 (ref. 22), functions together with the MALT1 adaptor protein[23,24] as a central regulator of TCR- and BCR-mediated NF-κB activation. In addition, it has been shown that NF-κB activation mediated by Bcl-10 and that MALT1 is also critical for FcεRI-induced cytokine production and late-phase anaphylactic reactions[25]. Thus, these studies indicate the possibility that the Bcl-10–MALT1 complex is critical for ITAM-mediated NF-κB activation in other type of cells as well as lymphocytes.

CARMA1 (also called CARD11 and Bimp3), a CARD-containing protein of the MAGUK (membrane-associated guanylate kinase) family, is essential for TCR- and BCR-induced NF-κB activation and acquired immunity through the regulation of protein kinase C (PKC)–dependent lipid raft recruitment of Bcl-10 and inhibitor of NF-κB (IκB) kinase (IKK) proteins[26,27]. The three adaptors, CARMA1, Bcl-10 and MALT1, thus interact with each other to form a complex, called the CARMA1–Bcl-10–MALT1 (CBM) complex. Involvement of the CBM complex in TLR4 signaling in B cells has been demonstrated[23,26,28].

CARD9 is structurally related to CARMA1 and is expressed in a variety of human tissues, including peripheral blood lymphocytes and spleen[29]. Like CARMA1, CARD9 associates with Bcl-10 through its CARD and synergistically induces NF-κB activation[29]. Analysis of *Card9*$^{-/-}$ mice has shown that CARD9 is involved in antifungal immunity[30]. CARD9 has been suggested to mediate signals from dectin-1 to NF-κB activation through its atypical ITAM and Syk, as *Card9*$^{-/-}$ macrophages show impaired NF-κB activation and cytokine production in response to zymosan and *Candida albicans*. However, it has been suggested that TNF production and NF-κB activation of macrophages after zymosan stimulation is dependent mainly on MyD88-mediated signaling[31]. Moreover, dectin-1 deficiency does not alter the production of TNF and IL-12 by macrophages and DCs after zymosan stimulation or the defense against *C. albicans*[32]. These reports suggest that the impairment of cytokine responses to zymosan and defense against *C. albicans* of *Card9*$^{-/-}$ mice is not simply due to impairment of the dectin-1–Syk–CARD9 signaling pathway. Therefore, the physiological functions of CARD9 in various innate immune responses remain to be determined. In addition, the functional relationship of CARD9 with CBM-mediated regulation needs to be defined to clarify CARD9-mediated signaling.

Here we report studies of *Card9*$^{-/-}$, *Card11*$^{-/-}$ (CARMA1-deficient) and *Bcl10*$^{-/-}$ mice showing that the signaling pathway through CARD9–Bcl-10 but not through CARMA1–Bcl-10 was essential for myeloid cell activation mediated by various FcRγ- and/or DAP12-associated receptors. Loss of either CARD9 or Bcl-10 abrogated ITAM-associated receptor–mediated inflammatory cytokine responses in macrophages and DCs because of impaired NF-κB activation. CARD9 deficiency impaired cytokine production through both dectin-1- and MyD88-mediated signaling pathways after zymosan stimulation in DCs. Moreover, the CARD9–Bcl-10 pathway was involved in various TLR responses in DCs but not in lymphocytes through the activation of mitogen-activated protein kinases (MAPKs). Although CARD9 was dispensable for TCR- and BCR-mediated acquired immunity, CARMA1 deficiency did not affect cytokine responses in myeloid cells mediated by ITAM receptors (that is, ITAM-associated and ITAM-bearing receptors) or TLRs. Thus, we provide here genetic evidence for differential requirements of CARD9 and CARMA1 in Bcl-10-mediated activation of myeloid cells and lymphoid cells, respectively.

RESULTS

Generation of CARD9-deficient mice

As with human CARD9 (ref. 29), bone marrow and spleen have very high expression of mouse CARD9, but it is barely detectable in thymus and lymph nodes, among the lymphoid organs (**Supplementary Fig. 1a** online). In the various hematopoietic cell populations, myeloid lineage cells such as macrophages, DCs and neutrophils have higher expression of CARD9 than do lymphocytes and mast cells (**Supplementary Fig. 1a**). To study the physiological function of CARD9, we generated CARD9-deficient (*Card9*$^{-/-}$) mice. As it has been shown that the CARD motif is an essential domain for Bcl-10–CARD9 interaction and NF-κB activation[29], we deleted exon 2 of mouse *Card9*, which encodes the CARD (**Supplementary Fig. 1b**). We confirmed gene targeting by Southern blot analysis (**Supplementary Fig. 1c**) and verified the null mutation of *Card9* by the absence of CARD9 by immunoblot analysis (**Supplementary Fig. 1d**). *Card9*$^{-/-}$ mice were born at the expected mendelian ratio and did not show any anatomic abnormalities.

CARD9 is dispensable for lymphocyte development and activation

Because CARD9 associates with Bcl-10 and Bcl-10 deficiency affects early thymic development, with more cells of the CD44$^-$CD25$^-$ subset in the CD4$^-$CD8$^-$ double-negative population[22], we first determined whether CARD9 deletion affected T cell development. *Card9*$^{-/-}$ mice had normal development of CD4$^-$CD8$^-$, CD4$^+$CD8$^+$, CD4$^+$CD8$^-$ and CD4$^-$CD8$^+$ cells in the thymus and of CD44$^+$CD25$^-$, CD44$^+$CD25$^+$,

$CD44^-CD25^+$ and $CD44^-CD25^-$ subsets in the double-negative populations (**Supplementary Fig. 2a** online). Moreover, the percentages (**Supplementary Fig. 2b**) and numbers (**Supplementary Fig. 2c**) of peripheral $CD3^+$ cells and of the $CD4^+$ and $CD8^+$ subsets of T cells were similar in *Card9*$^{-/-}$ and wild-type mice. As Bcl-10-mediated NF-κB activation is essential for T cell activation by TCRs, we next analyzed TCR-induced T cell activation in *Card9*$^{-/-}$ mice. *Card9*$^{-/-}$ T cells showed normal proliferation after stimulation with antibody to CD3 (anti-CD3) alone, with anti-CD3 plus anti-CD28 or with phorbol 12-myristate 13-acetate plus ionomycin (**Fig. 1a**). Consistent with those observations, the production of IFN-γ (**Fig. 1b**) and IL-2 (data not shown) and upregulation of the surface activation markers CD25, CD44 and CD69 (data not shown) after TCR stimulation were similar in wild-type and *Card9*$^{-/-}$ mice. Similarly, *Card9*$^{-/-}$ T cells had normal major histocompatibility complex–dependent responses to allogenic antigen-presenting cells (**Fig. 1c**) and the 'superantigen' staphylococcal enterotoxin B (**Fig. 1d**). These results demonstrate that CARD9 is dispensable for T cell development and TCR-mediated activation.

It has been reported that deficiency of Bcl-10, CARMA1 or MALT1 results in fewer mature $IgD^{hi}IgM^{lo}$ B cells and a lack of the $CD21^{hi}CD23^{lo}$ subset of marginal zone B cells in the spleen[23,26,28], suggesting that Bcl-10-mediated signaling is required for the peripheral differentiation of B cells. We therefore next examined whether CARD9 is involved in B cell development. B cell development in the bone marrow (**Supplementary Fig. 2d**) and numbers of $B220^+$ cells (**Supplementary Fig. 2e**) and $IgD^{hi}IgM^{lo}$ B cells and marginal zone B cells (**Supplementary Fig. 2f**) in the spleen were similar in *Card9*$^{-/-}$ and wild-type mice. As CARMA1–Bcl-10–mediated signaling is essential for BCR-, CD40- and TLR-induced B cell responses[22,23,26,28], we next analyzed the effect of CARD9 deficiency on B cell activation. The proliferation of splenic B cells after stimulation with anti-IgM (**Fig. 1e**), anti-CD40 (**Fig. 1f**), LPS or CpG DNA (**Fig. 1g**) was similar in *Card9*$^{-/-}$ and wild-type mice. Furthermore, *in vivo* antibody responses after immunization with the T cell–dependent antigen DNP-KLH (dinitrophenol–keyhole limpet hemocyanin) demonstrated normal production of DNP-specific IgM, IgG1, IgG2a and IgG3 in *Card9*$^{-/-}$ mice (**Fig. 1h**). These data

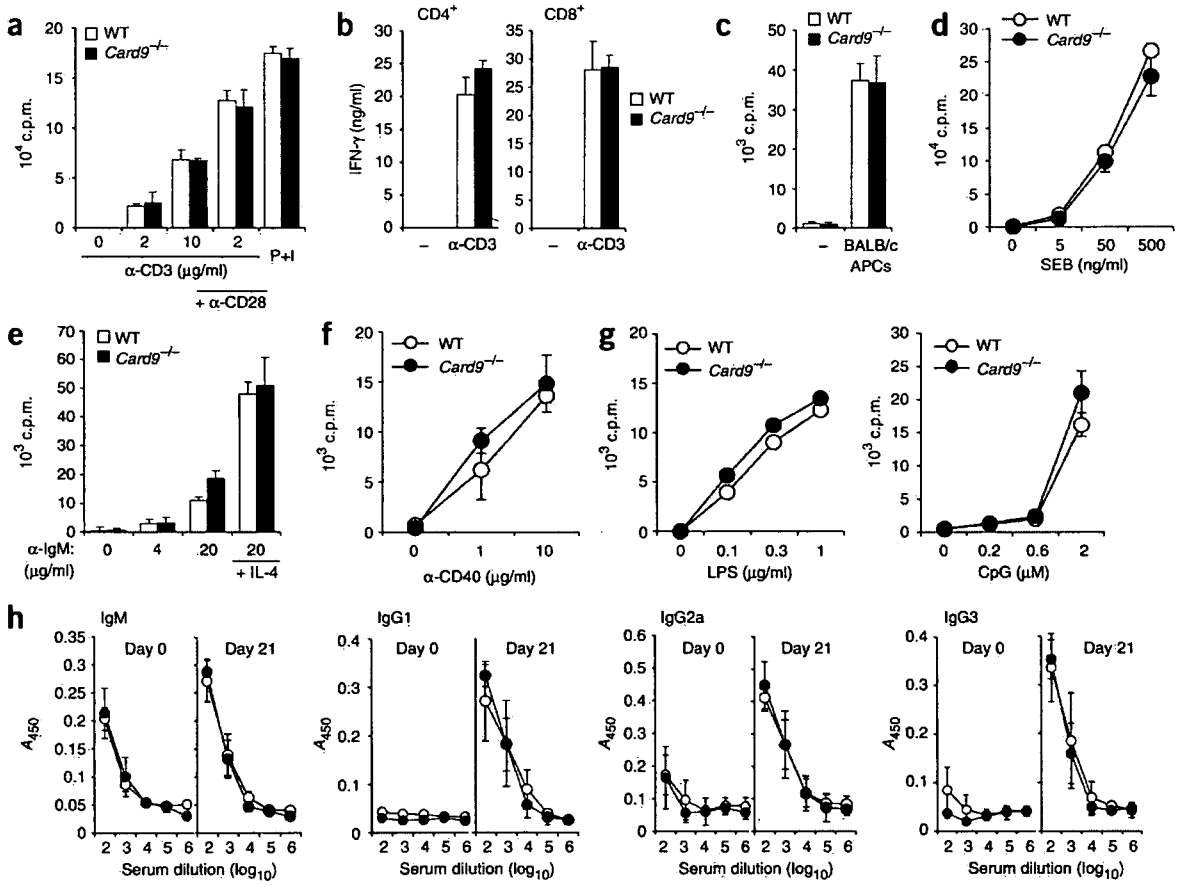

Figure 1 Normal activation of T and B lymphocytes in *Card9*$^{-/-}$ mice. (**a**) Proliferation of purified wild-type (WT) and *Card9*$^{-/-}$ T cells after stimulation with anti-CD3 alone (α-CD3; concentration, horizontal axis), anti-CD3 plus anti-CD28 (1 μg/ml; +α-CD28), or phorbol 12-myristate 13-acetate (10 ng/ml) plus ionomycin (1 μM; P+I). (**b**) ELISA of IFN-γ production by purified $CD4^+$ or $CD8^+$ lymph node T cells from wild-type and *Card9*$^{-/-}$ mice after 48 h of stimulation with anti-CD3 (α-CD3) or no stimulation (–). (**c**) Allogenic proliferative responses of wild-type and *Card9*$^{-/-}$ T cells after stimulation with irradiated spleen cells (APCs) from BALB/c mice or no stimulation (–). (**d**) Proliferation of T cells from wild-type or *Card9*$^{-/-}$ mice after stimulation with staphylococcal enterotoxin B (SEB) plus syngenic antigen-presenting cells. (**e–g**) Proliferation of purified wild-type and *Card9*$^{-/-}$ splenic B cells stimulated with the following: anti-IgM with (+ IL-4) or without recombinant IL-4 (10 ng/ml; **e**); anti-CD40 (**f**); LPS (**g**, left); or CpG DNA (**g**, right). (**h**) ELISA of serum titers of anti-DNP IgM, IgG1, IgG2a and IgG3 from wild-type mice (open circles; $n = 6$) or *Card9*$^{-/-}$ mice (filled circles; $n = 6$) immunized intraperitoneally with DNP-KLH on day 21 after immunization. A_{450}, absorbance at 450 nm. Data are the mean ± s.d. of triplicates (**a–g**) or six mice (**h**) and are representative of three (**a,b,e–g**), two (**c,d**) or one (**h**) independent experiment(s).